ELSEVIER

Contents lists available at ScienceDirect

International Journal of Heat and Mass Transfer

journal homepage: www.elsevier.com/locate/hmt



Shape optimization of hotspot targeted micro pin fins for heterogeneous integration applications



Najmeh Fallahtafti^{a,*}, Srikanth Rangarajan^a, Yaser Hadad^a, Charles Arvin^b, Kamal Sikka^b, Cong Hiep Hoang^a, Ghazal Mohsenian^a, Vahideh Radmard^a, Scott Schiffres^a, Bahgat Sammakia^a

ARTICLE INFO

Article history: Received 4 January 2022 Revised 17 March 2022 Accepted 3 April 2022 Available online 27 April 2022

Keywords:
Hotspot
Heterogeneous Integration
Multi objective optimization
Neural networks
Jet impingement
Thermal management
Liquid cooling
Electronics cooling

ABSTRACT

In the field of high-performance computing (HPC), growing power demands makes Heterogeneous Integration (HI) the future of next-generation computing systems to sustain Moore's law. HI refers to the assembly of different separately-manufactured components onto a single electronic module to enhance functionality and operating characteristics. As a consequence of HI, the next generation of electronic chips have regions of localized hotspots or cores, translating to a region of extremely high temperature if not adequately cooled. The mitigation of hotspots demands advanced thermal management cooling schemes compared to the conventional ones. This study investigates the combination of impingement jet array of liquid water and non-uniform hotspot targeted micro pin fins, printed on chips, as a potential heat transfer augmentation technique. The configuration comprises four $2cm \times 2cm$ chips (Total chip area is 16 cm²) with eight hotspots on each. Liquid water is employed as the coolant in the present study. A detailed numerical parametric study and optimization were carried out using a supervised machine learning algorithm. The multi-objective optimization is performed to optimize both the thermal and flow resistances simultaneously. The results from the detailed optimization reveal that optimal fin parameters for the regions of hotspot and background could be significantly different. The optimal pin fin configuration resulted in a minimum thermal resistance of 0.208 K.cm²/W (0.013K/W) at a constrained pressure drop of about 10 kPa.

© 2022 Elsevier Ltd. All rights reserved.

1. Introduction

Ever-shrinking size of electronic systems necessitates higher circuit integration per unit area, which, in turn, results in a rapid increase of heat generation per unit volume. Therefore, practical, efficient heat removal solutions that can make the system works in safe operating temperature and ensure its reliability have attracted researchers' attention for more than three decades [1–4]. The first step in developing much more effective heat removal solutions might be switching from air-cooling to hybrid and liquid-cooling [5]. Liquids with high specific heat capacity, thermal conductivity, density, and incompressibility, can absorb, store, and carry a larger amount of thermal energy than air on the way to replacing air cooling with liquid cooling. Much research was done on the characterization, and optimization of liquid-cooled heat sinks. Parallel microchannel heat sinks have been one of the practical so-

* Corresponding author.

E-mail address: nfallah1@binghamton.edu (N. Fallahtafti).

lutions for high power density application and studied extensively due to the high heat transfer surface area they provide at reasonable pressure drops. CFD simulation has been used for parametric study, hydraulic and thermal characterization, and heat transfer enhancement of parallel microchannel heat sinks used for uniform [3,6–8] and non-uniform [9] heat flux scenarios. Impingement micro channel heat sinks are becoming common because of their lower pressure drop, where there is no height restriction perpendicular to the electric board. Hadad et al. [10,11] studied the hydraulic and thermal performance of impingement microchannel water-cooled heat sinks numerically. Their results show that by replacing parallel microchannel heat sinks with impingement microchannel heat sinks, a considerable reduction in pressure drop is achievable without any significant thermal performance penalty.

Cooling of electronic systems is even more challenging when they benefit from heterogeneous integration (HI). Heterogeneous integration, as the basis of the future-generation computing systems refers to the assembly and placing separately manufactured

^a Department of Mechanical Engineering, State University of New York at Binghamton, Binghamton, NY, USA

b IBM Corporation, NY, USA

Nomenclature fluid specific heat capacity at constant pressure $c_{p.f}$ d_1 distance between two hotspots in a column (m) (Fig. 2(b)) d_2 hotspot columns distance (Fig. 2(b)) d_3 g_f^{HS} g_f^{BG} h_f^{HS} h_f^{BG} hotspot to chip edge distance (Fig. 2(b)) fin gap on hotspots (m) (Figs. 4 and 14) fin gap on back ground (m) (Figs. 4 and 14) fin height on hotspots (m) (Fig. 4) fin height on background (m) (Fig. 4) fluid thermal conductivity (W/m.K) k_f l_{chip} length of a chip (m) (Fig. 2(b)) PCBlength (m) (Fig. 2(a)) l_{PCB} length of a hotspot (m) (Fig. 2(b)) l_{HS} inlet length (m) (Figs. 4 and 7) l_{in} P pressure (Pa) p_{in} inlet pressure (Pa) outlet pressure (Pa) pout module total power (W) ġ Q flow rate (m^3/s) $q_{BG}^{\prime\prime}$ back ground heat flux (W/m^2) hotspot heat flux (W/m^2) $q_{HS}^{\prime\prime}$ R_{th} thermal resistance (K/W) R_{sp} t_f^{HS} t_f^{BG} spreading resistance (K/W)fin thickness on hotspots (m) (Figs. 4 and 14) fin thickness on background (m) (Figs. 4 and 14) chip thickness (m) (Fig. 4) t_{chip} die thickness (m) (Fig. 4) t_{die} inlet temperature (K) T_{in} temperature of the fluid (K) $T_{\rm f}$ T_s T_{max} temperature of the solid (K) chip maximum temperature (K) T_{min} chip minimum temperature (K) T^{die} max die maximum temperature at the bottom (K) T^{die} mean die mean temperature at the bottom (K) velocity field (m/s)w_{in} inlet width(m) (Figs. 4 and 7) outlet width (m) (Figs. 4 and 7) Wout W_{chip} width of a chip (m) (Fig. 2(b)) \mathbf{w}_{HS} width of a hotspot (m) (Fig. 2(b)) PCB width (m) (Fig. 2(a)) WPCB width of side wall's groove (m) (Fig. 4) Wg Greek symbols chip temperature non-uniformity (Eq. 7) ψ density of the fluid (kg/m^3) ρ_f absolute viscosity of the fluid (kg/m.s) μ_f

components on to a single electronic module. Heterogeneous integration improves system functionality by increasing its speed, and decreasing its power consumption, form factors, and weight [12–16]. High reduction in the size of electronic systems resulted from heterogeneous integration comes at the price of high heat flux and power density, which makes it challengeable for the conventional cooling technique like air-cooling and even liquid-cooled heat sinks with thermal interface material and heat spreaders. The problem becomes even more challenging when the system's heat sources have hotspots (non-uniform power map). On-chip hotspots are regions of excessively high heat flux, which have intense adverse effects on the electronic system performance, reliability and lifespan [17,18]. To address this difficult situation (cooling hetero-

geneous integrated electronic system involving on-chip hotspots), remedies with advanced knowledge behind them has been developed recently. Hotspot targeted heat sinks have proposed as an efficient remedy although they usually possess complicated architectures that are hard to manufacture. Ansari and Kim [18,19] proposed a microchannel pin fin hybrid heat sink with two separate zones. Micro channels were employed over the background, and cylindrical pin fins were utilized over the hotspots. This fin configuration increases convective heat transfer surface area on the top of the hotspots. A significant improvement in the thermal performance of the hybrid heat sink was observed compared to common microchannel heat sinks. Feng et al. [20] numerically and experimentally studied the effect of non-uniform distributed solid and annular-cavity micro pin fins on heat transfer and temperature uniformity of 3D-IC (three dimensional integrated circuits) chips including hotspots with 700 W/cm^2 . By providing adequate convection heat transfer surface area in the vicinity of regions on power concentration, Lorenzini et al. [21] and Sarvey et al. [22] mitigated the effect of hotspots at reasonable pressure drops. They divided the fin network to five zones with three different fin density according to heat flux and distance to hotspots. In order to increase the heat transfer surface area on the on-chip hotspots, Rubio-Jimenez et al. [23,24] suggested a novel micro pin fin heat sink with non-uniform fin density. They also studied the effect of fin cross section shape (circular, square, elliptical, and flat with redounded sides), fin length, and fin height on the temperature gradient at the base of the heat sink. Orthogonal thermal interface materials (TIM) and anisotropic heat spreaders are also considered as hotspot problem solutions. The application of these anisotropic systems is to spread the heat from small-area hotspots to the whole heat sink base area using high transverse thermal conductivity. Using analytical and numerical modeling Bachmann and Bar-Cohen [25] estimated the potential of anisotropic spreaders and TIMs to mitigate the hotspots. They showed that a reduction 30% in hotspot temperature is achievable by using anisotropic spreaders and TIMs together. Thermoelectric coolers have been used for hotspot alleviation although they suffer from high cost and low thermal efficiency. Hao et al. [26] suggested a solution of combining thermoelectric cooler (TEC) and minichannel heat sink to alleviate on-chip hotspots. They estimated TEC's performance under different boundary conditions using a theoretical model. They also studied the hotspot removal capability of TEC for different cooling conditions. Wang et al. [27] developed chip-level numerical simulations to predict the on-chip hotspot cooling capacity achievable with mini-contact TEC. Bulman et al. [28] show that a significant heat removal between 160 and 2500% is reachable by replacing common TECs with thin-film Bi₂Te₃-based super-lattice TECs.

Embedded cooling usually refers to cooling systems which bring the coolant in direct contact with the heat source (electrical chip). This technique becomes very efficient when the extended heat transfer surfaces attached directly to the heat source. Azizi et al. [29,30] showed how heat removal devices such as microchannels, micro pin fins, and vapor chambers can be directly printed onto silicon dies by employing selective laser melting (SLM) technology. They showed that a significant reduction in chip temperature for the silicon chip additive manufactured micro fins is achievable (compared with conventional heat sinks) as a result of the elimination of thermal interface material and heat spreader. Radmard et al. [31,32] numerically studied the performance of a cooling system of on-chip printed pin fins working with water. They investigated the effect of pin fin height profile on thermal resistance and pressure drop. Sharma et al. [33] employed an embedded liquid cooling technique (microchannels etched into a chip) for cooling a chip with a non-uniform power map. They designed an impinging manifold to target on-chip hotspots and optimized the micro channel structure.

Design of experiments (DOE) associated with CFD and different optimization algorithms have been extensively used for the optimization of thermal management systems with various applications. Rao et al. [34] employed Jaya algorithm for a dimensional optimization of a micro channel heat sink design parameters. They developed regression functions for thermal resistance and pressure drop of the heat sink to examine its performance. A multi-objective genetic algorithm was used by Kulkarni et al. [35] to optimize a double-layered micro channel heat sink. They used response surface method (RSM) to calculate regression functions for thermal resistance and pump power. Then, they optimized their heat sink by minimizing the regression functions of pressure drop and thermal resistance. Naqiuddin et al. [36] utilized Taguchi-grey method to optimize the design parameters of a segmented micro channel heat sink. Their objective was to minimize pressure drop and heat sink temperature gradient as well as maximizing specific performance (heat source power divided by the multiplication of the heat sink volume and its temperature difference) of the heat sink.

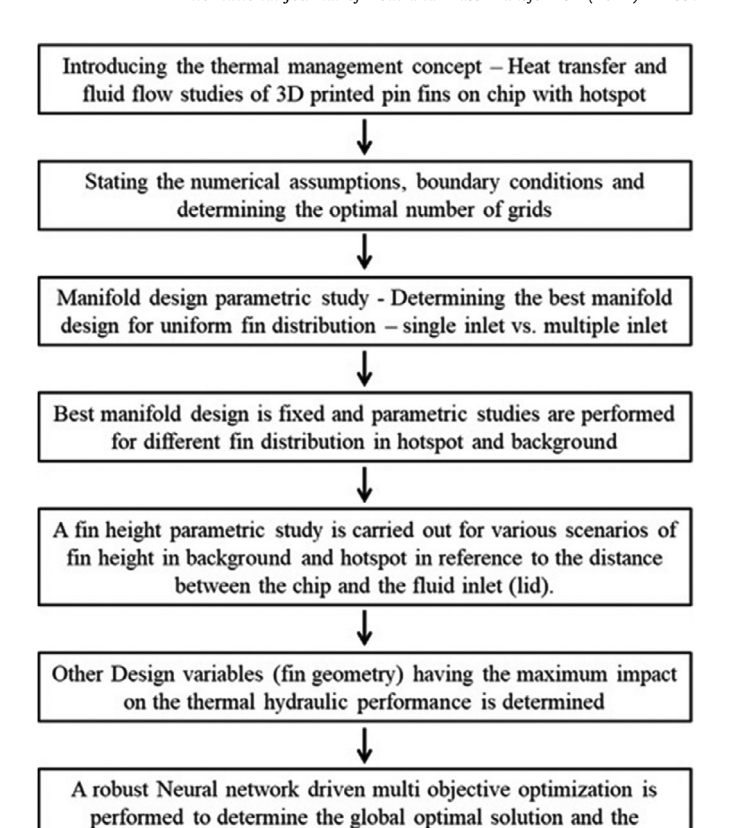
Machine learning algorithms have been applied by a few researchers to predict the thermo-hydraulic performance of the heat sink. Lee et al. [37] developed a multi-layer neural network model for predicting the hydraulic performance of a pin fin heat sink employed for high heat flux electronics using a huge amount of research data from the literature. The authors demonstrated that the ANN-based prediction of hydraulic performance was superior to the regression-based prediction. The authors employed a multilayer feedforward ANN and concluded that with a number of hidden layers =12, the best prediction was achieved. Xiang et al. [38] developed an Artificial Neural Network (ANN) for high accuracy prediction of cooling performance in the microchannel heat sink. The authors obtained the thermo-physical properties of the coolant (Liquid alloys) using the ANN and demonstrated the efficiency of ANN in estimating the best mass fraction of Indium that can maximize the cooling performance. Ghaedi [39] established an ANN model for simultaneous predictions of density, viscosity, thermal expansion coefficient, excess molar volume, and viscosity deviation of the aqueous solution of ethylene glycol monoethyl ether. Mohammadpour et al. [40] performed A comprehensive analysis consisting of computational fluid dynamics (CFD) and machine learning algorithms (MLAs) to study the effect of geometrical and operational parameters on nanofluid heat transfer in a microchannel heat sink (MCHS) with double synthetic jets (SJs). The authors concluded that The k-NN regression model shows more accurate predictions than the other MLAs

Rangarajan et al. [41,42] employed the supervised machine learning technique (Artificial Neural Networks) ANNs coupled with the Non-dominated sorted genetic algorithm NSGA-II to arrive at optimal designs for heat transfer problems. The authors demonstrated the superior efficiency of genetic algorithm and NSGA-II coupled with ANN over the other state of the art optimization algorithms.

The present work aims to achieve the following:

- Propose an efficient embedded cooling thermal management concept for high power heterogeneous integrated modules with on-chip hotspots
- Improving the performance of the initial proposed design (baseline) by using parametric study based on engineering intuition.
- Optimize the improved design by using modern optimization tools (Artificial Neural Network combined with Genetic Algorithm) with manufacturability constraints included.

In engineering problems, a detailed parametric study plays an important role in both the quality of the final optimized design and the amount of cost and time spent to reach it. Preliminary parametric study is a very powerful method which improves the



corresponding optimal design parameters.

Fig. 1. Research flow diagram.

initial design and at the same time makes the optimization process easier and more efficient by excluding low effective design parameters. In other words, parametric study helps engineers and designers to reduce the search space for optimization (Section 5).

The present study is organized as follows: Section 2 introduces the integrated electronic system and attached thermal management system in detail. Numerical analysis including governing equations, basic assumptions, computational domain and boundary conditions, and grid sensitivity analysis are brought in Section 3. Section 4 consists of parametric studies to improve the baseline and exclude low effective design parameters from optimization process. A parametric study is done in Section 4.1 on the system's manifold and first improvement in the design is achieved. In Section 4.2 a parametric study is performed on fin profile and the second enhancement is applied to the baseline. Section 4.3 provides a parametric study on the fin gap and thickness on the hotspot and background. Fin gap and thickness on the background is recognized as low effective parameters and removed from optimization process according to the results of this parametric study. A trade off study is presented in Section 4.4 for the final design parameters based on the modeling results obtained for optimization full factorial table. Finally, in Section 5, a robust Neural network driven multi objective optimization is performed to determine the global optimal solution and the corresponding optimal design parameters. Fig. 1 shows the path of this study in a flowchart for quick reference.

2. Problem description

2.1. Integrated electronic package

A schematic view of the electronic package including four chips setting on a PCB (printed circuit board) is shown in Fig. 2(a).

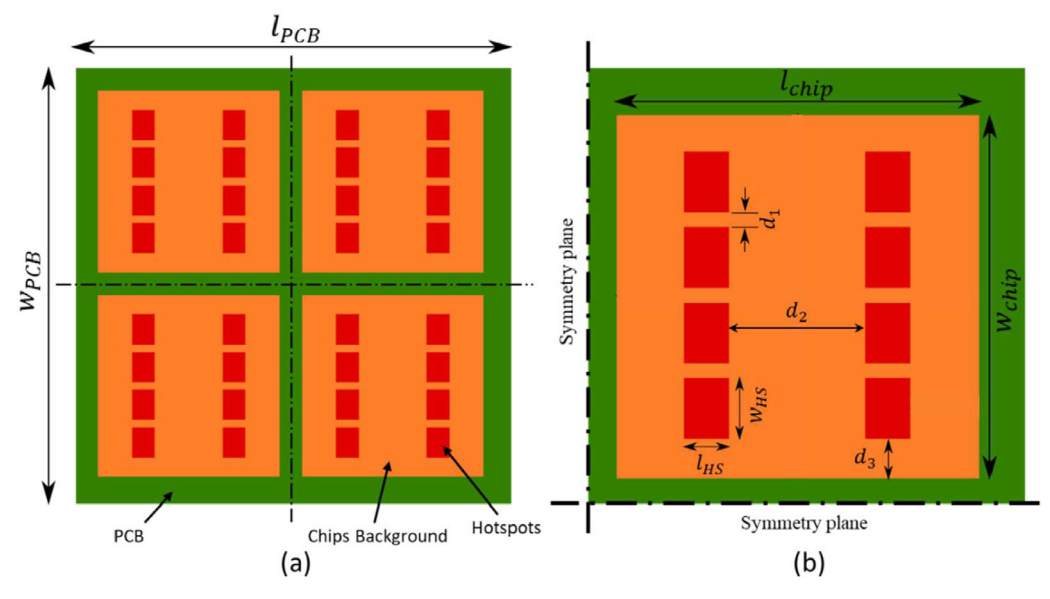


Fig. 2. (a) Schematic top view of the power map for the electronic HI Package of 4 chips. (b) The non-uniform power map of each chip with eight hotspots.

Table 1Geometric parameters of the electronic package.

Symbol	Definition	Value (mm)
$w_{chip} \times l_{chip}$	Chip size	20 × 20
$w_{PCB} \times l_{PCB}$	PCB size	48×48
$w_{HS} \times l_{HS}$	Hotspot size	3.35×2.5
d_1	Distance between two hotspots in a column	0.8
d_2	Hotspot columns distance	12.5
d_3	Hotspot to chip edge distance	2.1
t_{chip}	Chip thickness	0.1
t_{die}	Die thickness	0.4
t_{PCB}	PCB thickness	0.5

Table 2Operational parameters of the module.

Symbol	Definition	Value
\dot{q} $q_{BG}^{\prime\prime}$ $q_{HS}^{\prime\prime}$ $\dot{q}_{HS}^{\prime\prime}$ $\dot{q}_{HS}^{\prime\prime}/\dot{q}_{total}$ $q_{HS}^{\prime\prime}/q_{BG}^{\prime\prime}$	Module total power Background heat flux Hotspot heat flux Power ratio Hotspot to background heat flux ratio	4.14 (kW) 150 (W/cm ²) 800 (W/cm ²) 0.52 5.3
Q T _{in}	Flow rate Inlet temperature	8 <i>LPM</i> 293.15 (<i>K</i>)

Fig. 2(b) illustrates the non-uniform power map of each multicore chip. As shown in Fig. 2, each of the chips consists of eight hotspots (cores) arranged symmetrically in two columns. Design constraints are categorized to geometric and operational. The geometric parameters of the electronic package are displayed in Fig. 2 and listed in Table 1. The operational parameters are listed in Table 2. As seen, while hotspots occupy almost 17% area of the chips, they generate 52% of the total power.

2.2. Thermal management system

Fig. 3(a) shows an exploded view of the thermal management system's the initial design (baseline). As shown in Fig. 3(a), in the initial design micro pin fins with square cross section are uniformly distributed on the chips. The initial design possesses four single inlets located at the top of the chips. The dimensions of the baseline's fin network and manifold are provided in Table 3 and shown in Fig. 4. They are considered as design parameters

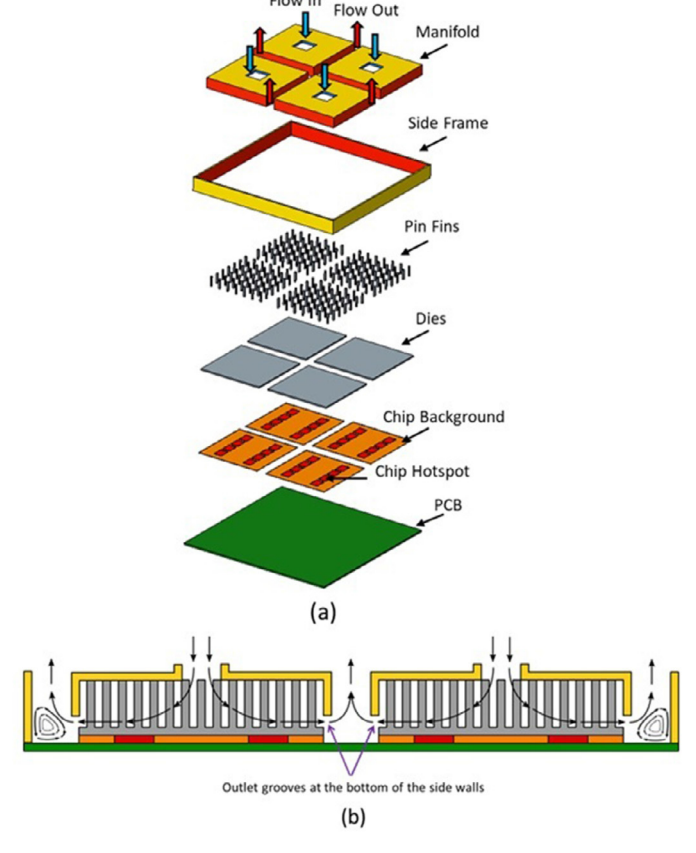


Fig. 3. (a) An exploded view of the thermal management system (b) Schematic view of coolant path in the module.

that vary in parametric study and optimization. The coolant is water entering the module at 20°C from top through impinging jets (Fig. 3(b)). The total coolant flow rate is fixed at 8LPM. Fig. 3(b) shows the path of the coolant throughout the module. As can be seen, after entering the module, coolant moves through the gaps between the fins and exits from the grooves created at the bottom of the side walls. Then, it turns by 90 degrees to the outlet ducts and exits the module.

Table 3Baseline's fin network and manifold dimensions.

Symbol	Definition	Value (mm)	
t gG	Fin thickness on background	0.4	
t ^{HS}	Fin thickness on hotspots	0.4	
ths gbg ghs ghs hg h ^{Hs}	Fin gap on background	0.2	
gHS f	Fin gap on hotspots	0.2	
h_f^{BG}	Fin height on background	3	
h ^{HS}	Fin height on hotspots	3	
$w_{in} \times l_{in}$	Inlet size	5 × 5	
w_{out}	Outlet width	2	
w_g	Width of side wall's groove	0.5	

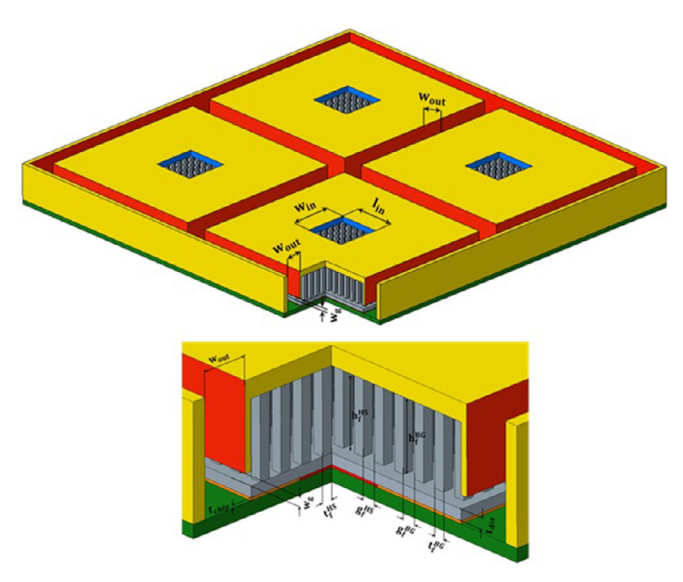


Fig. 4. Baseline's fin network and manifold dimensions.

3. Numerical analysis

3.1. Basic assumptions

Following assumptions are considered in solving the mass, momentum, and energy equations:

- 1. The flow field is three-dimensional, steady, incompressible, and single-phase.
- Flow is laminar everywhere (gaps, inlets, and outlets) as the flow field does not experience Reynolds number higher than 1500.
- 3. Gravity, radiation heat transfer, and viscous heat generation are negligible.
- 4. Thermo-physical properties of solid and fluid phases are constant.

It is worth mentioning that laminar model is used for numerical simulation according to the Reynolds number of inlet (< 1500), fin gap (\sim $O(10^1)$, and outlet ((\sim $O(10^2)$). Although impinging flows have high potential of creating vortices, they are not formed in the fin network of this study due to the low Reynolds number. In other words, high solid-fluid contact surface area (flow friction) and low velocity in the fin network make the momentum diffusion dominates momentum convection and damp flow field disturbance. In this study vortices are generated in the exit manifold shown in schematic of Fig. 3(b). Although vortices increase flow field disturbance, they are typically solved by laminar model in internal flow problems with Reynold numbers less than 1500 even if they are formed in heat sinks channels or fin gaps [21,43].

Table 4Thermo-physical properties of the coolant and solid phases.

	$\rho \ (kg/m^3)$	k (W/m.K)	c_p (J/kg.K)	μ (kg/m.s)
Silver	10500	406	230	-
Silicon	2330	149	700	-
Water	998.4	0.6028	4182.2	0.0010074

3.2. Governing equations

The governing equations (Eqs. (1-4)) for a 3D conductionconvection (conjugate) heat transfer problem in an incompressible, steady laminar flow regime are as follows:

Continuity (mass conservation) equation:

$$\nabla . \vec{V} = 0 \tag{1}$$

In which \vec{V} is the velocity vector field.

Navier-Stokes (momentum) equations:

$$\rho_f(\vec{V}.\nabla)\vec{V} = -\nabla P + \mu_f + \nabla^2 \vec{V} \tag{2}$$

Where ρ_f is the density of the fluid, P denotes the pressure field, and μ_f is the absolute viscosity of the fluid.

Energy equation for coolant fluid:

$$\rho_f c_{p,f}(\vec{V}.\nabla) T_f = k_f \nabla^2 T_f \tag{3}$$

In Eq. (3) $c_{p,f}$ represents the fluid specific heat capacity at constant pressure, T_f is the temperature of the fluid, and k_f stands for fluid conductivity.

The energy equation for solid phases:

$$\nabla^2 T_{\rm s} = 0 \tag{4}$$

Where T_s represents the temperature of the solid phase.

3.3. Material properties

The numerical simulation consists of two distinct solid phases, silicon and silver. Micro pin fins are printed in silver on the surface of the silicon chip. The coolant is water with an inlet temperature of 20°C. The thermo-physical properties of the coolant were assumed constant and were obtained from thermodynamics tables at the inlet temperature. Table 4 shows the thermo-physical properties of the solid phases and the coolant. It is worth mentioning that FR4 (Glass-reinforced epoxy laminate material) is considered for the PCB material.

3.4. Numerical domain and boundary conditions

In this study, the presence of the hotspots causes a highly nonuniform heat flux boundary condition. Therefore, the smallest computational domain that satisfies both the geometry of the interest and the heat flux boundary conditions is one fourth of the module (one chip).

Fig. 5 shows the computational domain with associated boundary conditions. Symmetry (zero gradient) planes are shown in red dash lines. The coolant enters the module from the top through the "velocity inlets" and exits it from "pressure constant" slots placed on the lid (Fig. 5). Adiabatic and no-slip boundary conditions are imposed on the side walls and the lid. No-slip and thermally coupled boundary conditions are applied to the lateral surfaces of the fins and the top of the die which are in touch with coolant and exchange heat. Constant heat fluxes are imposed to the chip background and the hotspots as shown in Fig. 5.

3.5. Numerical approach

The fluid dynamics and heat transfer modeling were performed using 6SigmaET, which is part of the 6SigmaDCX software package.

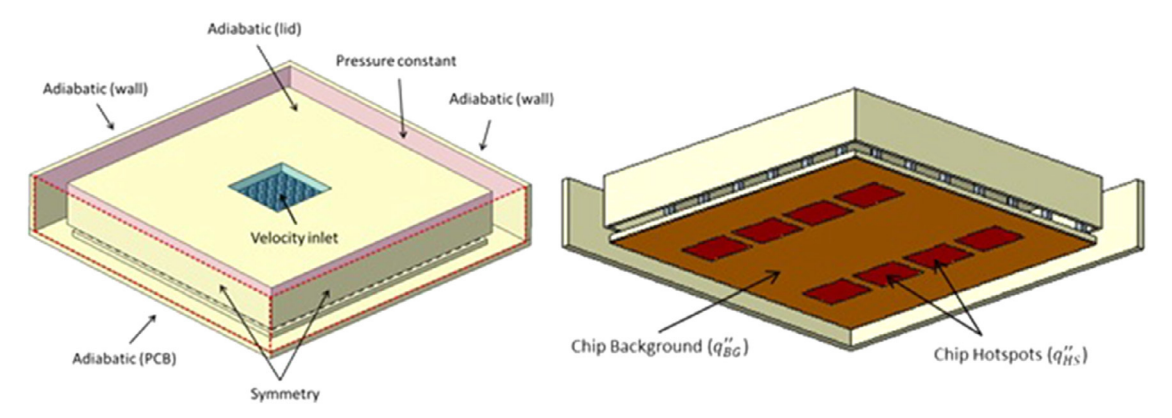


Fig. 5. Schematic view of the computational domain with associated boundary conditions.

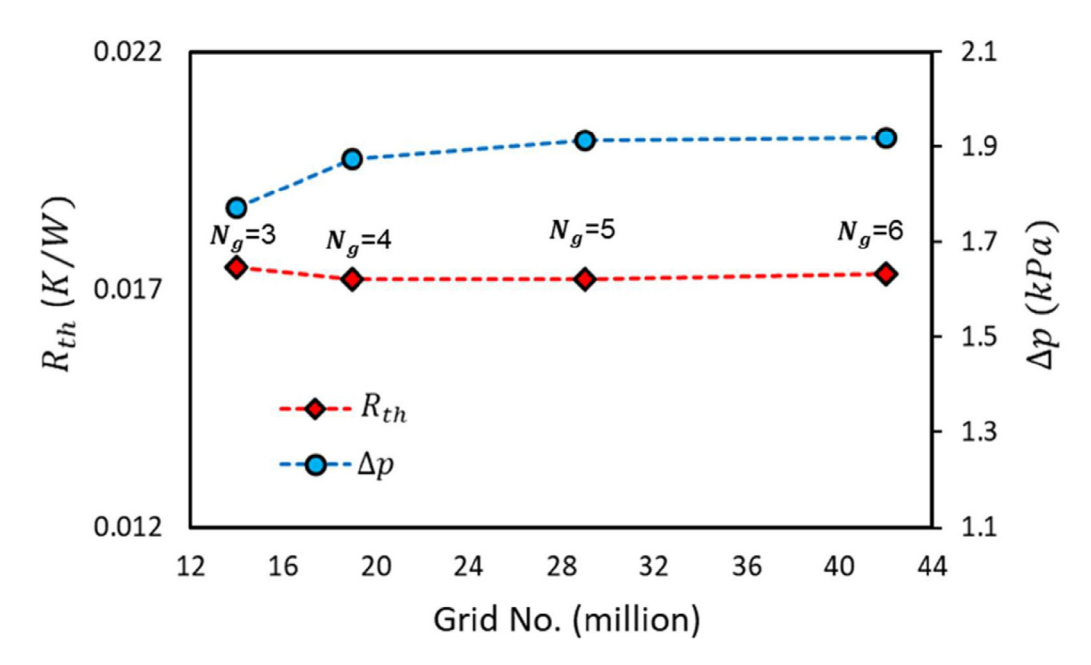


Fig. 6. Grid sensitivity analysis graph for the baseline design.

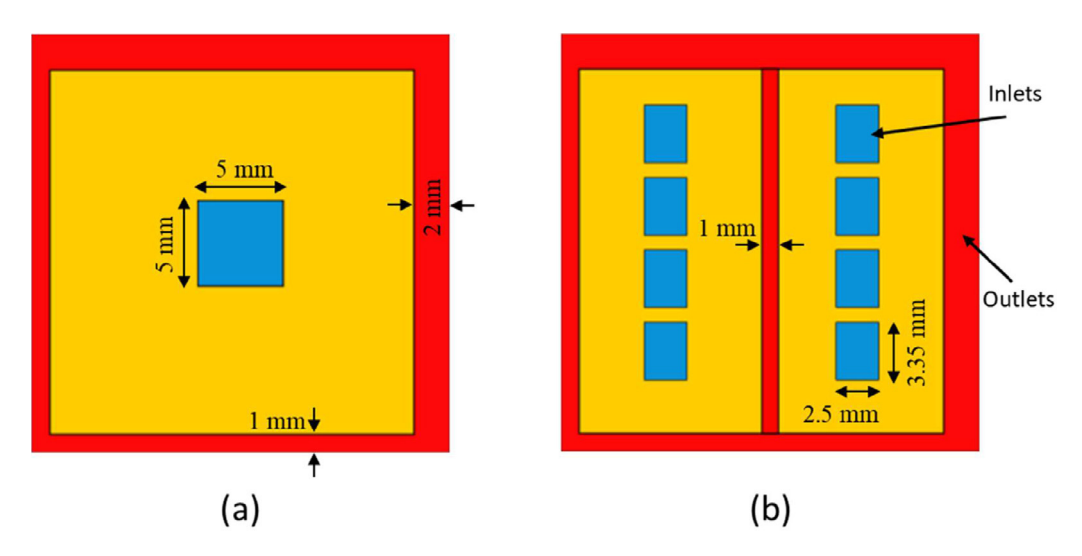


Fig. 7. (a) Single-inlet (b) Multi-inlet manifold designs. Inlets are illustrated in blue and outlets are shown in red.

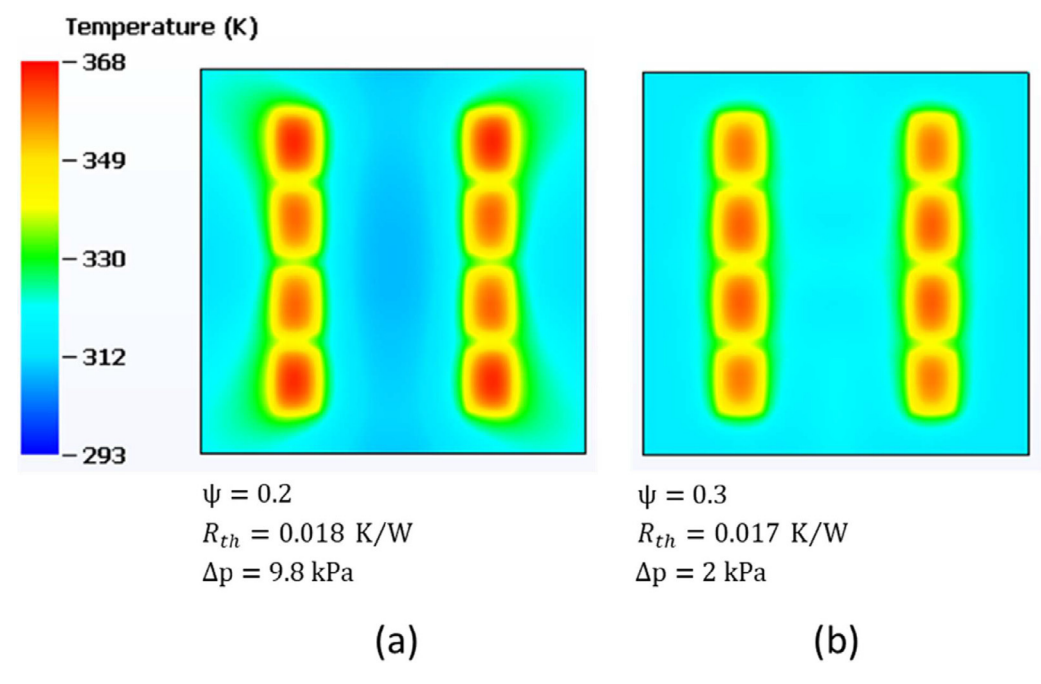


Fig. 8. Chip temperature profiles for (a) single-inlet manifold and (b) multi-inlet manifold.

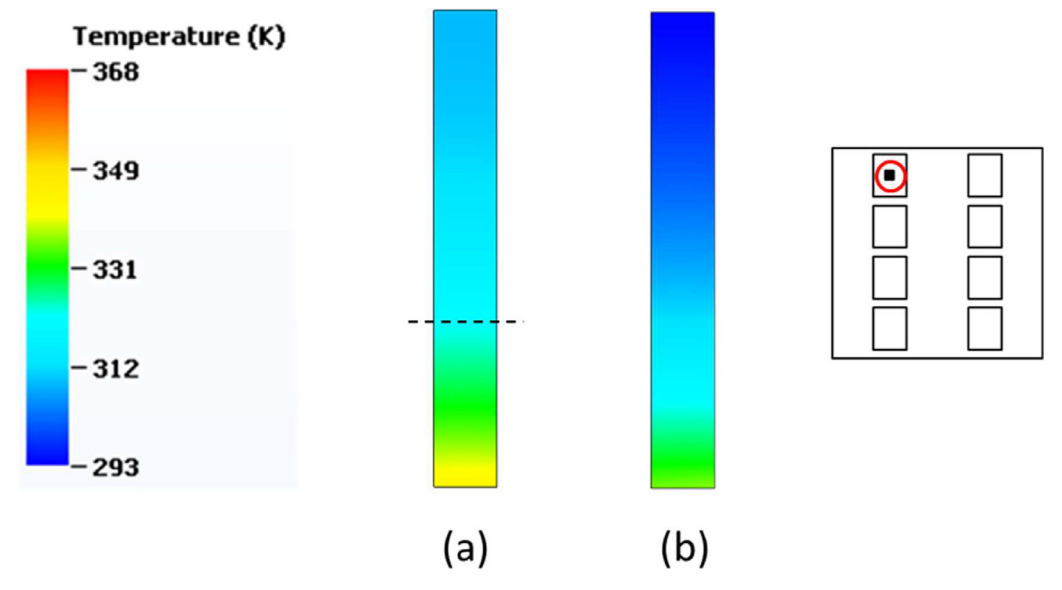


Fig. 9. Hotspot fin temperature profile for (a) single inlet and (b) multi inlet manifolds.

This package uses the finite volume method (FVM) to discretize the system of governing equations (Continuity, Navier-Stokes, and Energy equations) in the computational domain on a staggered grid. All of the module components (distributor, collector, and micropin fin network) were modelled as a single package. In order to calculating the fields of velocity, pressure, and temperature, the system of governing equations was solved using iterative SIMPLE algorithm. To accurately capture the pressure drop and heat transfer at this scale, 6SigmaET's MLUS (multi-level unstructured solver) was employed. The mathematical formulation of this method employs a hierarchy of Cartesian grids and a face-to-cell connectivity graph to discretize the differential equations [44]. The method uses a finite volume scheme with staggered variable arrangement and a pressure-based segregated iteration procedure to solve a discrete algebraic analogue of the momentum equations (Navier-Stocks equations). The method provides accuracy and robustness like the structured procedure and is more flexible in resolving complex geometries and different solution scales. With the unstructured grid providing the necessary resolution of the geometrical details, the model exhibits a substantial reduction in the number of computational cells.

3.5.1. Grid sensitivity analysis

The number of cells varies from one design to another owing to fin thickness, gap, and height. Fin gaps which are under the inlets and on the hotspots are regions of high velocity and temperature gradients. In order to capture the thermal and hydraulic boundary layers in these regions by numerical solution, number of cells in fin gaps is considered as a grid sensitivity analysis criterion. For the baseline, and full factorial designs of optimization process, the total number of cells changes between 19 and 168 million depending on the fin network geometry. The grid sensitivity analysis was performed based on the system pressure drop and thermal resistance defined by Eqs. (5) and (6).

$$R_{th} = \frac{T_{max}^{die} - T_{in}}{\dot{q}} \tag{5}$$

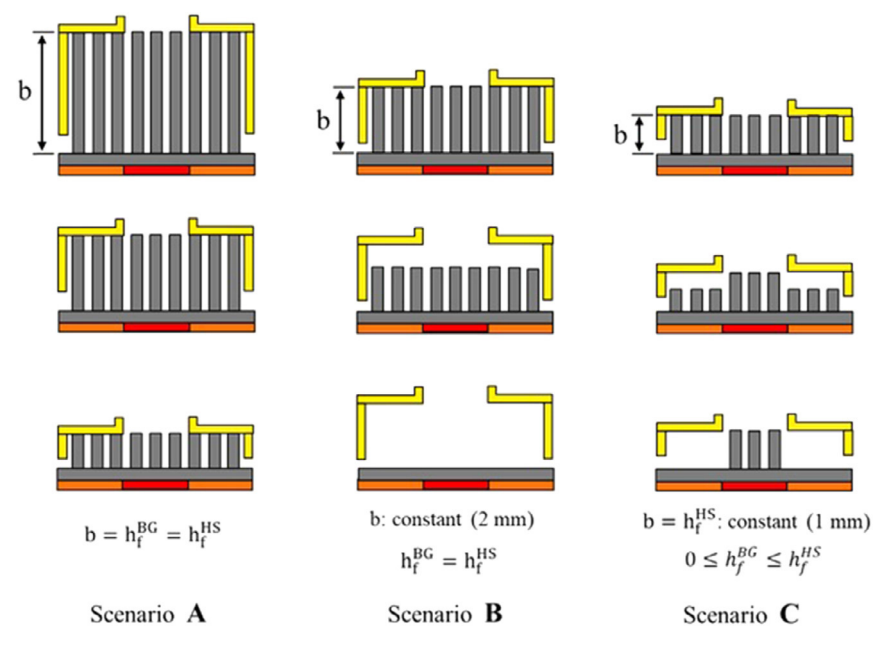


Fig. 10. Schematics of three fin profiles for fin height parametric study.

In which T_{max}^{die} is maximum temperature of the die at its bottom. T_{in} denotes the coolant inlet temperature and \dot{q} represents module total power.

$$\Delta P = P_{in} - P_{out} \tag{6}$$

 P_{ln} and P_{out} are pressure at the inlet and outlet, respectively. The result of this study for the baseline with a fin gap of 0.2 mm is illustrated in Fig. 6. The figure shows the variation of thermal resistance and pressure drop with total grid number. The number of cells between two fins are also mentioned next to each point. As shown in Fig. 6 the discrepancy of thermal resistance and pressure drop does not exceed 2% from second to third grid number. From third to forth grid number both thermal resistance and pressure drop almost level off. Thus, the second grid (19 million cells) is selected for the baseline geometry.

4. Parametric study

4.1. Manifold design parametric study

The performance of cooling system is evaluated for single-inlet (baseline) and multi-inlet manifolds. In the single-inlet system, a jet of size $5 \times 5 \text{ mm}^2$ impinges the flow to the center of each chip (Fig. 7(a)). In the multi-inlet scenario, eight jets in the size of the hotspots impinge the coolant directly to the top of them (Fig. 7(b)). Besides, one outlet slot with the width of 1 mm is embedded in the center of the lid (Fig. 7(b)). In Fig. 7, blue and red colors represent system inlets and outlets, respectively. It should be mentioned that, in this study, the thermo-hydraulic performance of the cooling system is assessed by thermal resistance (Eq. (5)) and pressure drop (Eq. (6)). A remarkable reduction of 79% (from 9763 Pa to 1972 Pa) and a slight change of 5.5% (from 0.018K/W to 0.017K/W) are observed in pressure drop and thermal resistance, respectively by replacing the single inlet with jets at the top of the hotspots. Chip temperature uniformity is another thermal response parameter that is affected by the manifold architecture. The more uniform temperature profile a chip has, the less thermal stress it experiences resulting in longer lifespan. Chip temperature profiles for the two manifold designs (single and multiple inlets) are compared in Fig. 8. As Fig. 8 demonstrates, chip temperature profile is more uniform in the multi-inlet manifold compared with the single-inlet manifold. In order to show it quantitatively, the parameter ψ is defined as a measure of chip temperature uniformity as follows:

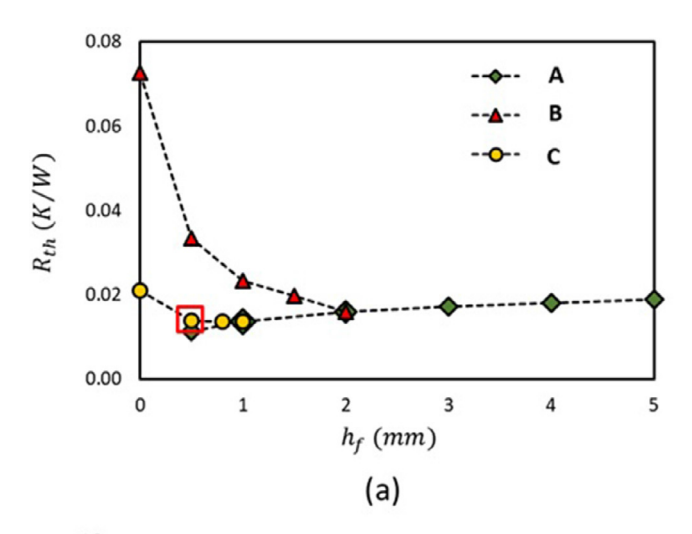
$$\psi = \frac{T_{\min}^{\text{chip}} - T_{\text{in}}}{T_{\max}^{\text{chip}} - T_{\text{in}}} \tag{7}$$

The parameter ψ varies between zero and one. Obviously, when ψ is equal to one $(T_{max}^{chip} = T_{min}^{chip} = T_{ave}^{chip})$ the chip is ideally isothermal. Chip temperature gradient increases as ψ approaches to zero. The values of ψ offered by single and multi-inlet manifolds are calculated as 0.2 and 0.3, respectively. Indeed, an increase of 50% in chip temperature uniformity is observed by switching from single-inlet to multi-inlet manifold. Here, the first improvement is applied to the baseline by replacing its single-inlet manifold by multi-inlet manifold with inlets on the top of the hotspots. Fig. 9 compares the temperature profiles for a fin on one of the hotspots in two scenarios of single and multi-inlets. As the figure shows, approximately one-third of the fin participates in heat transfer in single inlet scenario. This is quite different in multi inlet scenario where more than two-third of the fin is involved in heat transfer and brings the hotspot in lower temperature.

4.2. Fin height parametric study

The effect of the fin height on the cooling system performance is investigated for three fin height profiles shown in Fig. 10. The fin height is uniformly cut from 5 mm to 0.5 mm with no gap between fin tip and the lid in profile (A). In profile (B) the lid is fixed at the height of 2 mm while the fin height decreases from 2 mm to 0 mm (no fin). Profile (C) presents a full fin height of 1 mm on the hotspots and shorter fins (0 $\leq h_f^B \leq 1$) on the background.

Fig. 11 (a) shows that in profile (A) the thermal resistance continuously decreases as the fins are shorten from 5 mm to 0.5 mm (by 42%). From one side, shortening the fins decreases fin thermal resistance and increases coolant flow velocity (Reynolds number) in the gaps which result in cooling system's thermal resistance reduction. On the other side, reducing the fin height reduces the heat transfer surface area which increases thermal resistance. A gradual reduction in cooling system's thermal resistance in profile (A)



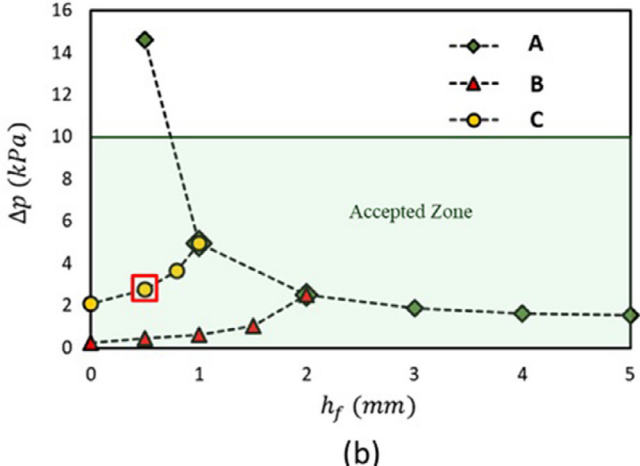


Fig. 11. (a) Thermal and (b) Hydraulic performance of three fin profiles (A), (B), and (C).

with shortening the fins shows that the effect of higher coolant velocity and lower fin thermal resistance dominate the impact of heat transfer surface area reduction. Fig. 11 (b) shows that by cutting the fins from 5 mm to 1 mm the pressure drop constantly rises due to the higher flow velocity between the fins. The rate of pressure rise with fin height reduction increases as pressure drop is proportional to fluid velocity square. A sharp jump of 200%, over the accepted zone ($\Delta p < 10kPa$), is observed from the height of 1 mm to 0.5 mm. Although the thermal resistance of the fin height of 1 mm is slightly higher than that of 0.5 mm, its pressure drop is three times smaller. Thus, $h_f = 1$ mm is considered as the optimal fin height for profile (A).

At the next step of fin height parametric study, in order to investigate the effect of gap between fin tip and the lid, the distance of the inlets (lid) from the root of the fins is fixed to (2 mm) and fin height uniformly varies from 2 mm to zero (profile (B)). As Fig. 11 (a) shows, the thermal resistance incredibly rises to 4.5 times from the fin height of 2 mm to no-fin module. In profile (B), reducing the fin height decreases heat transfer surface area and gap flow velocity simultaneously. This decreases convection heat transfer and results in a dramatic upsurge in thermal resistance. However, the pressure drop follows a reverse trend as demonstrated in Fig. 11 (b) due to the lower gap flow velocity and liquid-solid contact surface area. It falls down to one-tenth in no-fin module compared to 2 mm fin height. It is worth mentioning that, in profile (B), as fin height decreases a part of the flow skips the fins

Table 5 Initial ranges of variation of design parameters.

Design Parameters	Ranges of Variation (mm)
t_f^{HS} t_f^{BG}	0.3 - 0.6
t_f^{BG}	0.2 - 0.4
g ^{HS}	0.1 - 0.4
g _f g _f g _f	0.2 - 0.5

through top to the exit grooves as this path offers lower flow resistance. By comparing the thermal resistances of the profiles (A) and (B), it can be observed that gapless profile (A) outperforms profile (B) with a gap between the tip of the fins and the lid. Therefore, the profile (B) is refused for optimization due to its poor thermal performance.

In profile (C), the full fin height of 1 mm is maintained on the hotspots and fins on the back ground are cut from 1 mm to zero (Fig. 10). Fig. 11 (a) and (b) show that by cutting the fins on the back ground from 1 mm to 0.5 mm, the thermal resistance remains almost constant. It stems from the fact that the thermal resistance of non-uniform power map systems is mainly determined by elevated heat flux zones (hotspots). Consequently, reducing the heat transfer surface area on the low heat flux zones (background) does not affect the thermal performance of the systems significantly. As it is expected, the pressure drop shows a remarkable reduction (44%) by cutting the fins on the background as it decreases both gap flow velocity and resistance there. Although a 24 % reduction in pressure drop happens from fin height of 0.5 mm to no-fin on the background, there is a jump of 50 % in thermal resistance due to the minimum possible heat transfer surface area. Here, the second improvement in the baseline design resulted from fin height parametric study is applied by keeping full fin height of 1mm on the hotspots and 0.5 mm on the background. This design is distinguished by red squares in Fig. 11. Improvements of 70% and 17% are observed in temperature uniformity and thermal resistance, respectively relative to the first-improved design (uniform fin profile with multiple inlets). However, a 40% rise in pressure drop occurs due to the shorter fin network and consequently higher flow velocity between the fins. Fig. 12 shows temperature profiles of these two designs. As it is expected, non-uniform fin profile design brings the chip in more uniform temperature (and lower maximum temperature) as it prioritizes hotspots to cool.

Fig. 13 shows the temperature distributions of a hotspot fin for uniform fin height and non-uniform fin height profiles (both with multi-inlets). As the figure shows, unlike in uniform fin height profile, in non-uniform fin height profile the whole of the hotspot fins take part in the heat transfer as they are shorter and possess lower thermal resistance.

4.3. Fin gap and thickness parametric study

Four design parameters, fin thickness and gap on the background (t_f^{BG}, g_f^{BG}) and the hotspots (t_f^{HS}, g_f^{HS}) are considered for channel network optimization. Fig. 14 shows a schematic of fins on a hotspot and part of the background from top view. Thermal resistance and pressure drop are optimization response parameters for thermal and hydraulic performance, respectively.

Initial ranges of variation are determined for design parameters (shown in Table 5) according to what is common in literature [45–50] and manufacturability. Previous studies [3,9,32,51] done for uniform heat flux, declare that thick fins with narrow gaps enhance heat transfer. This knowledge is considered in establishing initial ranges of variation for design parameters. Furthermore, a parametric study is conducted on the bounds of initial design parameters.

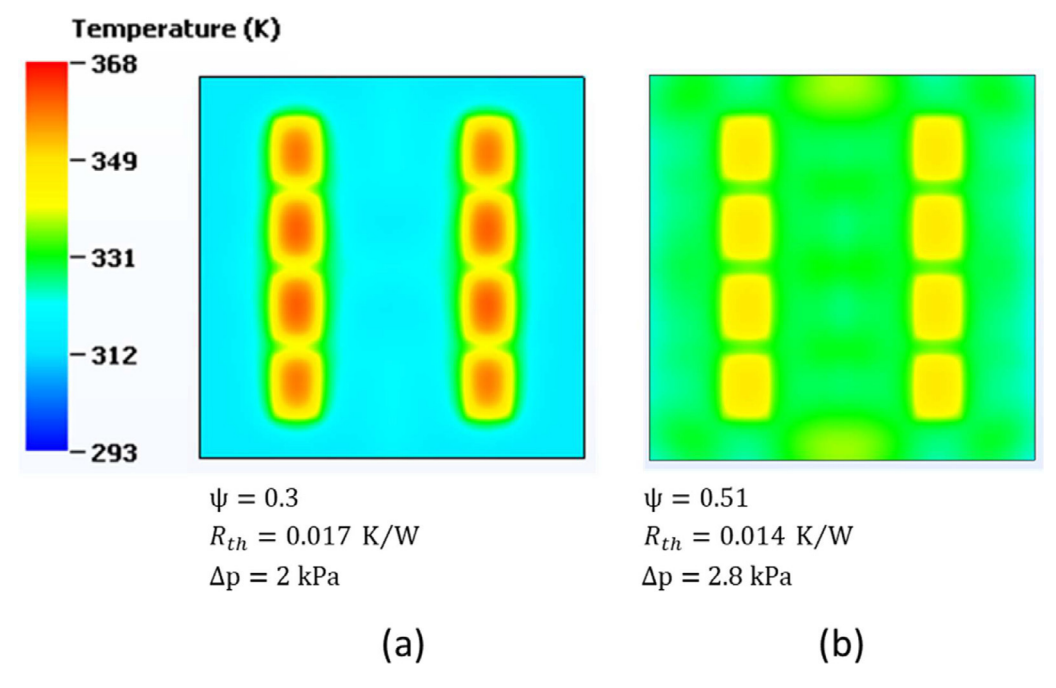


Fig. 12. Chip temperature profiles for (a) first improved design (uniform fin profile with multiple inlets) and (b) second improved design (non-uniform fin profile with multiple inlets).

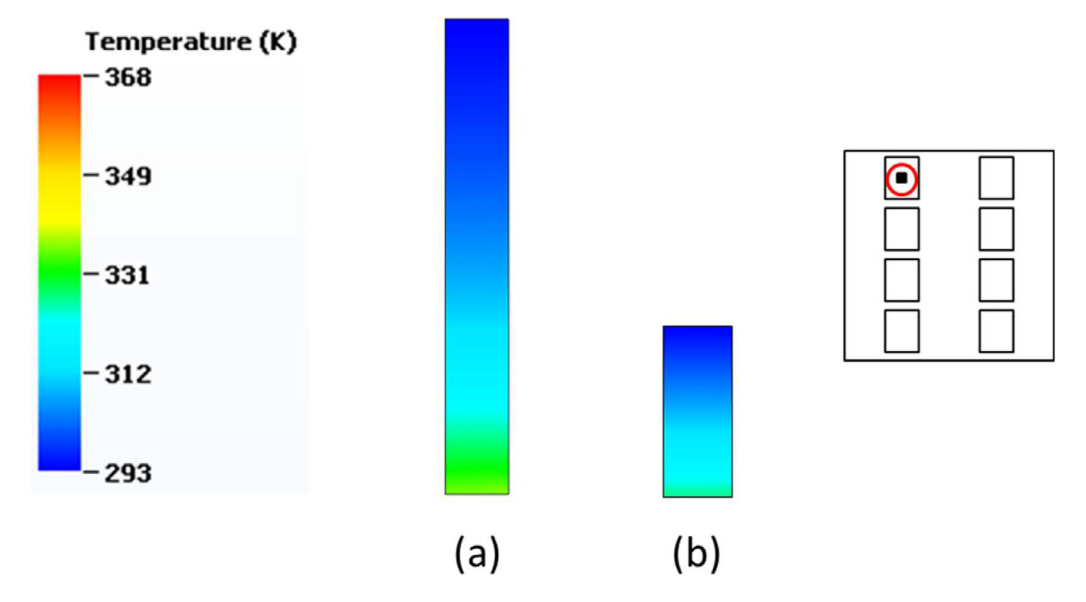


Fig. 13. Hotspot fin temperature profile for (a) first improved design (uniform fin height with multiple inlets) and (b) second improved design (non-uniform fin height with multiple inlets).

rameters ranges. Eight permutations of the bounds are considered for this parametric study shown in Table 6.

Fig. 15 (a) shows thermal resistances of the eight designs. The results are categorized by the value of fin gap on the hotspots. As can be seen, thermal resistance does not change considerably as long as g_f^{HS} is fixed regardless of the background fin configuration. Thermal resistance jumps by 50 % when g_f^{HS} increases from 0.1m to 0.4m. It is concluded that thermal performance of the cooling system mainly depends on the value of the gap between the fins on the hotspots. The background geometry does not affect the thermal performance remarkably because in the proposed cooling system, heat is removed from the chips locally based on the power map and the system does not possess a heat spreader.

Fig. 15 (b) demonstrates pressure drop for six permutations of Table 6 categorized in three fin configurations on the hotspots

 $(g_f^{HS},\ t_f^{HS})$. Comparing these three categories, it is concluded that the pressure drop mainly depends on the fin configuration on the hotspot. Comparing the first category (designs NO. 1 & No.2) to the second category (designs NO.3 & NO.4) with the same fin gap on the hotspots, one concludes that fin thickness on the hotspot has a significant effect on the system pressure drop. The same conclusion is obtained for fin gap on the hotspot by comparing second (designs NO.3 & NO.4) and third (designs NO.7 & NO.8) categories in Fig. 15 (b). Here, like thermal performance, the hydraulic performance does not show significant dependence on background fin configuration as fin array on the background is shorter (than that on the hotspots) and the flow easily skips it to the exit grooves. Therefore, the fin configuration on the background is fixed with $t_f^B = 0.2\ mm$ and $g_f^B = 0.5\ mm$ because of slightly lower pressure drop compared to the other background fin configuration ($t_f^B = 0.5\ mm$).

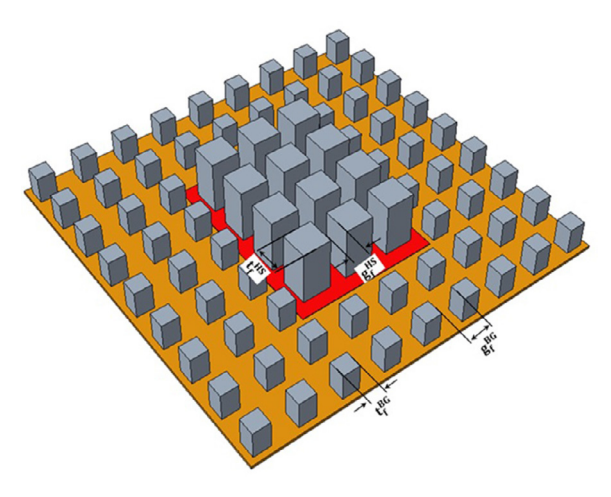


Fig. 14. A schematic of fin distribution on a hotspot and back ground.

Table 6Designs evaluated at the bounds of the variables considered in the study.

Design NO.	$t_f^{BG}(mm)$	$t_f^{HS}(mm)$	$g_f^{BG}(mm)$	$g_f^{HS}(mm)$
1	0.4	0.6	0.2	0.1
2	0.2	0.6	0.5	0.1
3	0.4	0.3	0.2	0.1
4	0.2	0.3	0.5	0.1
5	0.2	0.2	0.5	0.1
6	0.2	0.5	0.5	0.1
7	0.4	0.3	0.2	0.4
8	0.2	0.3	0.5	0.4

Table 7Final design parameters with associated ranges of variation (fin thickness and gap on the background are fixed to 0.2 and 0.5, respectively).

Design Parameters	Ranges of Variation
t ^{HS} f g ^{HS} g ^F	0.2 - 0.6 0.1 - 0.4

 $0.4\ mm$ and $g_f^B=0.2\ mm$). Here, the number of optimization design parameters is reduced from four to two by applying a parametric study to them. Working with two design parameters (instead of four) simplifies the optimization process and makes it easier to solve more design points (full factorial with five levels for each parameter) which results in more accurate optimization. Table 7 shows the final optimization design parameters with associated ranges of variation.

4.4. Trade-off analysis (full factorial design)

A full factorial design (FFD) table (Table 8) is developed based on two design parameters, t_f^{HS} and g_f^{HS} . Five levels are considered for each design parameter. Therefore, 25 fin network designs are solved and the results are demonstrated in Fig. 16. The variation of the thermal resistance of the cooling system with fin thickness on the hotspots are demonstrated in Fig. 16 (a) for different values of fin gap on the hotspots. Thermal resistance decreases with fin thickness (t_f^{HS}) at high values of fin gap (e.g. $g_f^{HS} = 0.4 \ mm$). By increasing the thickness of fins on hotspots their thermal resistance decreases while the total hotspots convective heat transfer surface area does not change significantly (Fig. 16 (a)). This results in the total thermal resistance reduction of the cooling system. The total heat transfer surface area of designs with $g_f^{HS} = 0.1 \ mm$,

Table 8 Full factorial design table.

Design NO.	$t_f^{HS}(mm)$	$g_f^{HS}(mm)$	$R_{th}(K/W)$	$\Delta p(Pa)$
1	0.4	0.1	0.014	7129
2	0.6	0.4	0.023	5000
3	0.2	0.4	0.028	1177
4	0.4	0.4	0.023	2373
5	0.6	0.25	0.019	6025
6	0.2	0.1	0.014	3351
7	0.4	0.25	0.019	3076
8	0.6	0.1	0.014	13149
9	0.2	0.25	0.021	1483
10	0.2	0.175	0.018	1869
11	0.2	0.325	0.025	1269
12	0.3	0.1	0.013	5152
13	0.3	0.175	0.017	3010
14	0.3	0.25	0.020	2244
15	0.3	0.325	0.022	2005
16	0.3	0.4	0.026	1651
17	0.4	0.175	0.017	4267
18	0.4	0.325	0.022	2766
19	0.5	0.1	0.014	9908
20	0.5	0.175	0.017	5633
21	0.5	0.25	0.018	4626
22	0.5	0.325	0.020	3794
23	0.5	0.4	0.024	3485
24	0.6	0.175	0.017	7894
25	0.6	0.325	0.020	5452

 $g_f^{HS}=0.4~mm$, and $t_f^{HS}=0.2~mm$ is shown on Fig. 16 (a) close to their points. The sensitivity of thermal resistance on t_f^{HS} decreases by reducing g_f^{HS} , as for $g_f^{HS}=0.1~mm$, thermal resistance is not a function of t_f^{HS} any more. Indeed, in narrow fin gap designs like $g_f^{HS} = 0.1 \text{ mm}$ increasing the thickness of fins on hotspots from one side decreases fin thermal resistance and on the other side reduces the hotspots convective heat transfer surface area (demonstrated on Fig. 16 (a)). The effect of these changes cancels each other out, which results in a flat trend of system thermal resistance versus fin thickness on the hotspots (t_f^{HS}). As Fig. 16 (a) shows, thermal resistance drops with decreasing fin gap at constant fin thickness on the hotspots. By decreasing fin gap at a fixed fin thickness (e.g. $t_f^{\rm HS} = 0.2 \ mm$), gap flow velocity and convective heat transfer surface area increase simultaneously which result in thermal resistance reduction (path A-B on Fig. 16 (a)). Fig. 16 (b) illustrates the variation of pressure drop with t_f^{HS} and g_f^{HS} . As expected system's pressure drop increases with fin thickness at constant fin gap because of a growth in liquid-solid contact surface area and lower available entrance area. The pressure drop increases by reducing fin gap at constant fin thickness due to simultaneous growth in gap velocity and the liquid-solid contact surface area.

Fig. 17 compares the fin temperature for the designs with highest thermal resistance ($g_f^{HS} = 0.4 \, mm$, $t_f^{HS} = 0.2 \, mm$) and lowest thermal resistance ($g_f^{HS} = 0.1 \, mm$, $t_f^{HS} = 0.3 \, mm$) of FFD Table. As Fig. 17 shows, in the design with narrow gaps, fins work in a lower temperature range (308–320 K) than the design with wide gaps (356–368 K). It can be also seen, as opposed to the wide gap design, the narrow gap design has its hotspot fins totally participating in the heat transfer.

Heat spreading affects chip maximum temperature and temperature uniformity when cooling non-uniform power chips. In these cases, heat spreading occurs in chip, die, and heat sink base. Sarvey et al. [22] studied the effect of heat spreading in chip and heat sink base on the thermal performance of a chip with a hotspot in its center. They studied a liquid cooled heat sink with more heat transfer surface area concentrated in the vicinity of the hotspot. Their results show that while heat spreading through the base can

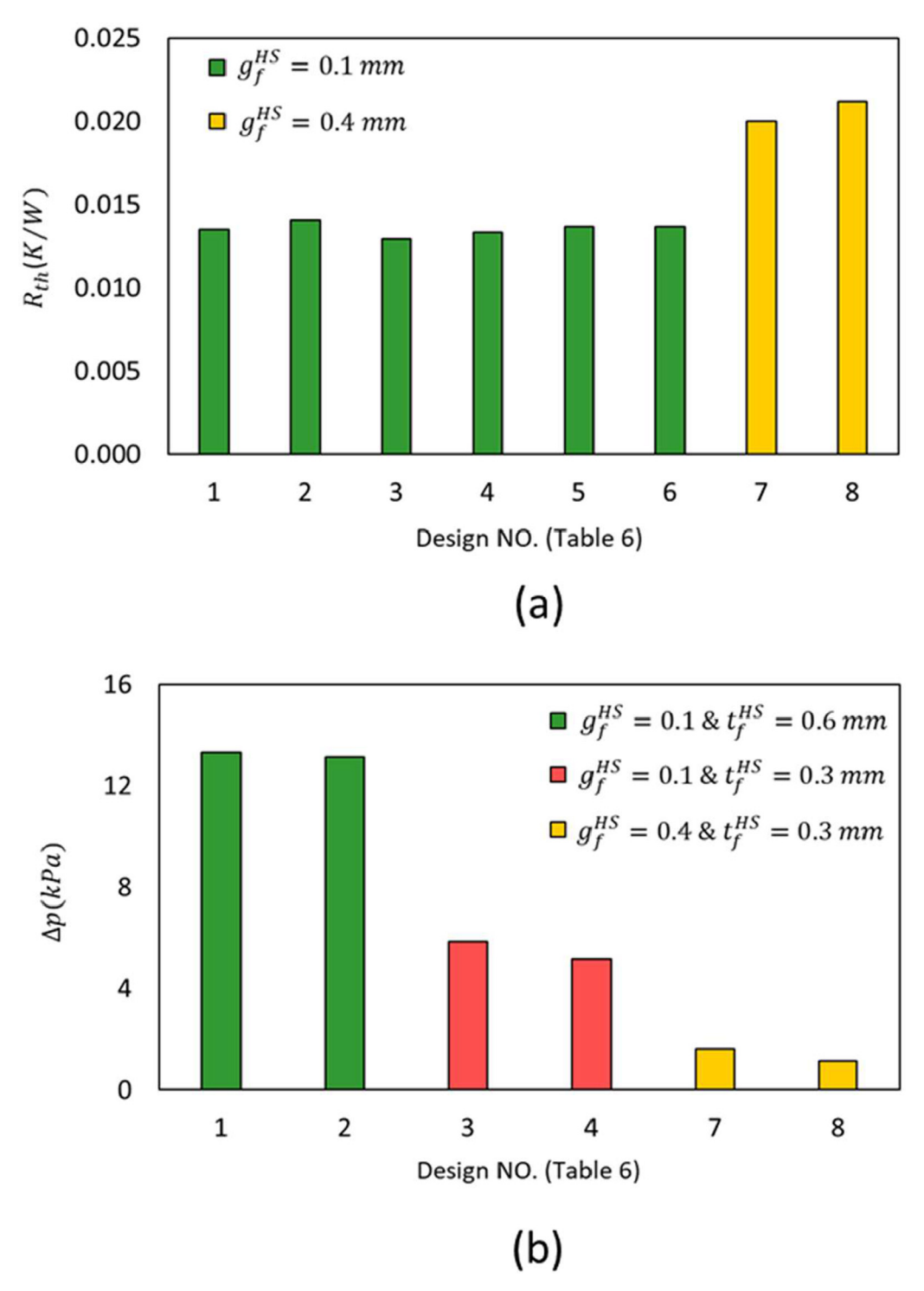


Fig. 15. (a) Thermal resistance and (b) pressure drop for fin gap and thickness parametric study.

decrease hotspot temperature with uniform cooling, spreading increases the temperature in the cases with enhanced cooling over the hotspot. As in this study an enhanced cooling system with fin and coolant flow concentration on the hotspot is used to alleviate the effect of hotspots, heat spreader has been removed. In the present cooling scenario, heat spreading takes place in the thin (0.4mm) layer of silver die which is printed on the chip uniformly and then pin fins are printed on it. In order to have an overall view of the heat spreading in the current system, die spreading resistance, defined by Eq. (8) is calculated for four DOE designs with

extreme fin and gap dimensions shown in Fig. 18.

$$R_{Sp} = \frac{T_{max}^{die} - T_{mean}^{die}}{\dot{q}} \tag{8}$$

In Eq. (8) T_{max}^{Die} and T_{mean}^{Die} are maximum and mean temperature at the bottom of the die.

As Fig. 18 shows for both fin gap of 0.4mm and 0.1mm the spreading resistance follows the trend of system total thermal resistance. This result is expected as the die maximum temperature (in the numerator of Eqs. (5) and (8)) is determined by fin configu-

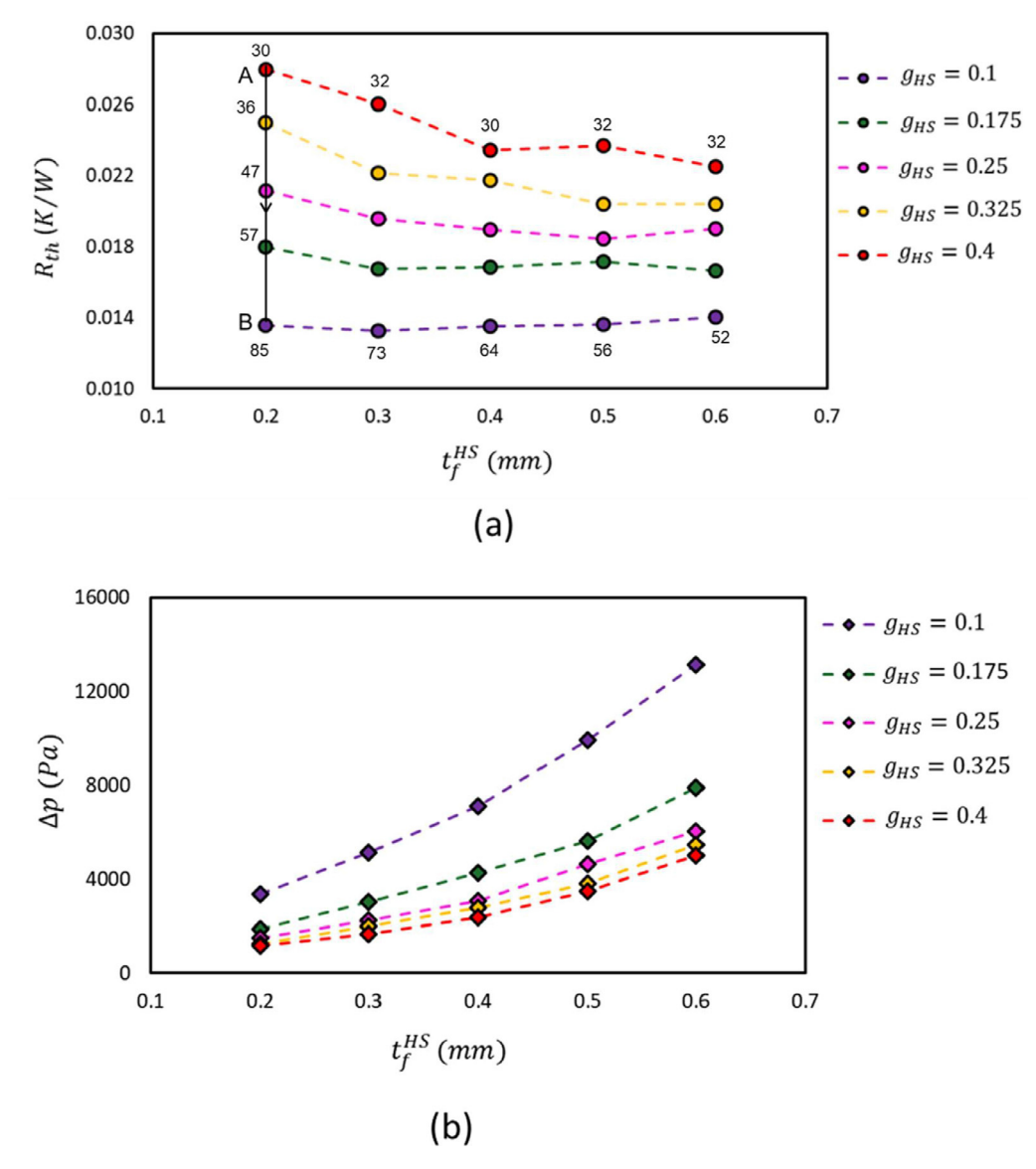


Fig. 16. (a) Thermal resistance (the numbers next to the points are heat transfer surface area on each hotspot in mm^2) and (b) pressure drop variations with hotspot fin thickness and gap in full factorial design points.

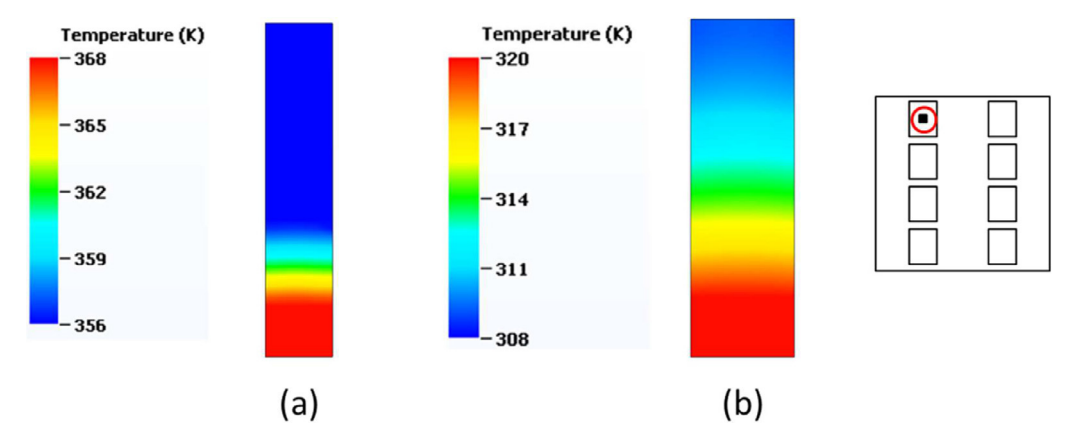


Fig. 17. Hotspot fin temperature profiles of the FFD designs with (a) highest and (b) lowest thermal resistances.

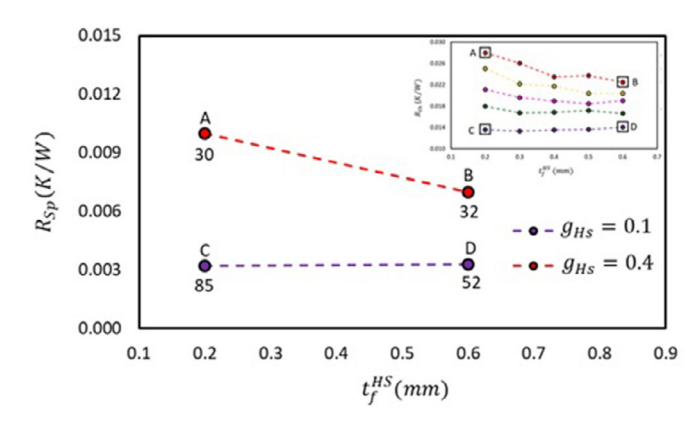


Fig. 18. Spreading resistance for four designs (A, B, C, and D) with maximum and minimum fin thickness and gap.

ration on the hotspot. Die mean temperature is affected by hotspot and background temperature. Background possesses the same fin configuration in all designs. For design points of A and B with $g_{Hs}=0.4\ mm$ spreading resistance is almost 35% and 33% of the total thermal resistance. The spreading resistance in designs C and D has a contribution of about 24% in system total thermal resistance.

5. Physics driven learning-based optimization

The optimization of the fin geometries was carried out using the supervised learning-based algorithm employing artificial neural networks (ANN) coupled with the state-of-the-art non-dominated sorting genetic algorithm -II (NSGA-II). The results from all the numerical cases were fed as an input in to the neural network. A neural network is a machine learning algorithm inspired by the model of a human brain/neuron. A neural network implemented in this study contain the following 3 layers:

- Input layer The activity of the input units represents the raw information that can feed into the network. This is the layer where the physics-based data from the numerical simulations are fed. The number of neurons in the input layer is the same as the number of input variables.
- Hidden layer In this layer the information is processed by employing the activations functions. The tan sigmoid function is employed as the activations function. The number of neurons in this layer is critical to determine the efficiency of the algorithm.
- Output layer The behavior of the output units depends on the activity of the hidden units and the weights between the hidden and output units. The backpropagation algorithm is employed to check the correctness of the output with the actual data available.

For highly efficient learning, the neural network demands highly diverse data for the problem under consideration. The diversity of the data should include

- (i) Design points from the bounds of the variables considered in the study
- (ii) Design points that can help generalize the physics of the problem

Though from the initial parametric study we see a monotonic variation of response parameters with respect to a particular design variable while other variables are fixed, a complete learning of the physics with all variables from models A, B and C (shown in Fig. 10) considered simultaneously becomes essential to obtain global optimal solutions.

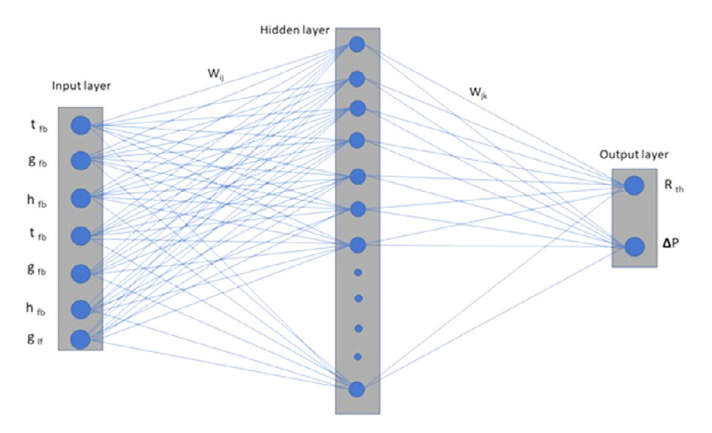


Fig. 19. Architecture of the network employed in the present study. The blue circles indicate the neurons in each layer.

The architecture of the network employed in the study is as shown in Fig. 19. As seen in Fig. 19, Wij and Wjk represent the weight matrix between the input hidden layer and the hidden output layer. The size of the weight matrices determines the complexity or the non-linearity of the problem under consideration. The number of neurons in the hidden layer (n_h) determines the size of the weight matrices for a fixed number of input and output layers. The procedure to determine the n_h is elucidated in the forthcoming discussions.

The training of the network was carried out using the Bayesian regularization method [52,53]. Interested readers can refer to the articles [52,53] to understand the background of the learning algorithm. The objective of the Bayesian regularization method is to minimize the combined error function and the weight function.

$$F = Min(\beta E_D + \alpha E_w)$$

Where.

 $E_{\text{\scriptsize D}}$ is the sum of squares error (SSE) between the data from the physics and output of the network

Ew is the sum of squares of network weights

The choice of values of the objective function parameters β and α is fixed to resolve the trade-off between network fitting and smoothness of the data, respectively. For highly nonlinear data, α and β are given equal weightage. The process of reducing the E_w is termed as the regularization. The regularization process is achieved by employing the Levenberg Marquadt algorithm by minimizing the gradient of the Hessian matrix that comprises the Jacobians. Minimizing the Hessian matrix minimizes the size of the weight matrices.

The procedure for ANN in this study is as follows:

- (a) Selection of input and output parameters for the neurons in the input and output layer respectively. The variables employed in each of the layers are shown in Fig. 19.
- (b) Dividing available data collected from the physics based CFD simulations into three types namely training, validation and testing data sets. The physics-based data collected from the CFD model provided input for the network, 89% of which were allocated to the training, and 11% of which were employed to evaluate the network. 5 sets of data outside the neural network were employed to test the robustness of the network.
- (c) Normalization of the data was done in the range of [-1, 1] as the tan hyperbolic function has its limiting values in the range [-1, 1].
- (d) Setting proper transfer functions for all layers.

A hyperbolic tangent function was introduced into the hidden layers.

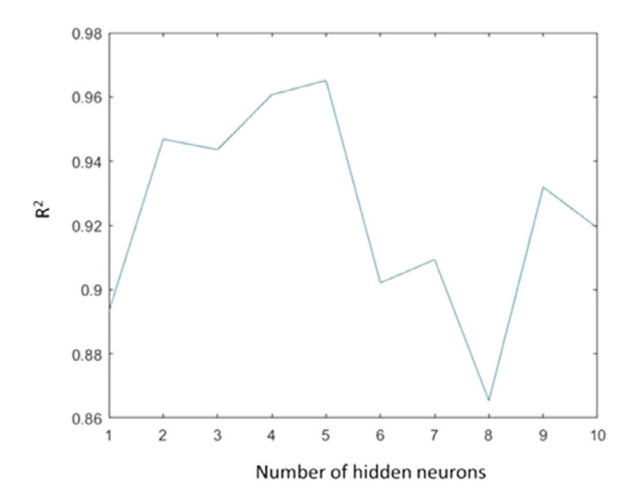


Fig. 20. Results of the neuron independent study.

- (a) Determining the optimal number of neurons using the neuron independent study. The most important part of the Bayesian based learning process is to determine the optimal number of hidden neurons that can increase the accuracy of the fitting and minimize the number of variables in the learning process. To minimize the number of variables in the learning process, the number of weights involved has to be kept minimum. The number of weights is dependent on the number of input neurons/variables, output neurons/variables and number of hidden neurons. As the number of input/output variables are fixed in the study, determining the number of hidden neurons is done by neuron independent study. A neuron independent study is performed to determine the optimal number of neurons in the hidden layer that maximizes the coefficient of determination R² as shown in Fig. 20. It is evident from the results that $n_h = 5$ corresponds to maximum R^2 . This is a valuable result as the network achieved maximum R² with minimum n_{h_h} Henceforth the network with $n_h = 5$ was employed for the optimization study.
- (b) Testing the network output. The results of the network fitting are shown in Fig. 21. The results from the parity plot makes it evident that the error due to data is highly minimized and shows good agreement with the physics of the problem. Furthermore, the network was tested for its robustness by testing the network for additional points and the agreement between the data and the network was exceptionally good. Henceforth the developed learning-based network was employed for the multi objective optimization study.

The non-dominated sorting Genetic Algorithm- II developed by Deb et al. [54] was employed for the optimization study. Srikanth et al. [41,55] applied the algorithm to a variety of heat transfer problem and demonstrated the Pareto optimal solutions. Rangarajan and Balaji [42] also concluded that among the various multi objective optimization algorithms for heat transfer problems, NSGA-II gave the best results in terms of diversity and closeness to the true optimal solution.

Maximum number of generations was fixed to 500. However, it was observed that the algorithm converged to the Pareto optimal in 130 generations. A. sensitivity study was performed on the probability of crossover on the final solution. The diversity of the solution was chosen as the performance metric. It was observed that when the probability of crossover was increased beyond 0.6 the results did not show significant changes. The Pareto optimal solu-

tions obtained are as shown in Fig. 22. The optimal solutions obtained showed excellent agreement with the physics-based model data (error less than 2%) that was initially employed to train the network. As shown in Fig. 22, the optimal solutions are predominantly a function of the hotspot fin geometry. The background fin geometry and hotspot fin geometry are less interactive to achieve minimum thermal resistance. This is also true from the physics point of view as there is very minimum or negligible heat spreading from the hotspot region to the background, indicating that the optimal solution depends on the convection solution (fin + flow) on top of the hotspot. To conclude, the optimal solutions and the learning-based algorithm represent and generalize the physics of the problem under consideration, respectively. The optimal solutions obtained were validated by a detailed CFD model as discussed in Section 4 and an excellent agreement was obtained. The maximum error was found to be within 2%.

Fig. 23 compares the chip temperature profiles for non-uniform fin design obtained in Section 4.2 and final optimal design. A slight improvement in thermal resistance of 7% and an improvement of 22% in chip temperature uniformity are obtained throughout the optimization with a penalty of pressure drop of 85% that is still reasonable and significantly lower than the maximum allowable value (10 kPa).

Fig. 24 compares hotspot fin temperature profiles for the last improved design in Section 4.2 pre-optimized design) and the final optimal design. As the figure shows, in the optimal design the hotspot fins offer higher fin performance and involve in heat transfer more than the pre-optimized design.

6. Conclusions

In the present study, we numerically demonstrated a novel energy-efficient thermal management solution using a combination of impingement jet arrays of liquid water and configuration of hotspot targeted micro pin fins that are directly printed on the chip surface. A physics-informed learning-based algorithm was developed for the problem under consideration. A robust multi-objective optimization algorithm was performed and the Pareto optimal solutions were obtained. The proposed cooling scheme demonstrates potential high benefits in mitigating on-chip hotspots. The major conclusions from this study are

- As opposed to the conventional cooling solutions (cold plates), the proposed thermal management solution does not involve TIM and heat spreader, which significantly improves its thermal performance.
- ii. The thermal performance of a non-uniform power map system is mainly determined by the fin configuration and geometry on the elevated heat flux zones (hotspots). This is the reason that the calculated optimal fin configuration is non-uniform. Indeed, the hydraulic performance of the system substantially benefits from small amount of extended heat transfer surface on the background.
- iii. By using a primary parametric study on the design parameters, their number were reduced from four (fin thickness on the hotspot, fin thickness on the back ground, fin gap on the hotspot, and fin gap on the back ground) to two (fin thickness and gap on the hotspot). Indeed, a primary parametric study was used to eliminate less influential parameters and make the optimization process more efficient.
- iv. The thermal performance of the system shows highest sensitivity to the fin gap on the hotspot (g_f^{HS}). For a fixed flow rate, the thermal resistance monotonically decreases by decreasing the fin gap on the hotspot regions.
- v. The sensitivity of the system thermal performance (thermal resistance) to fin thickness on the hotspot (t_f^{HS}) decreases by

15

Non trained data

10

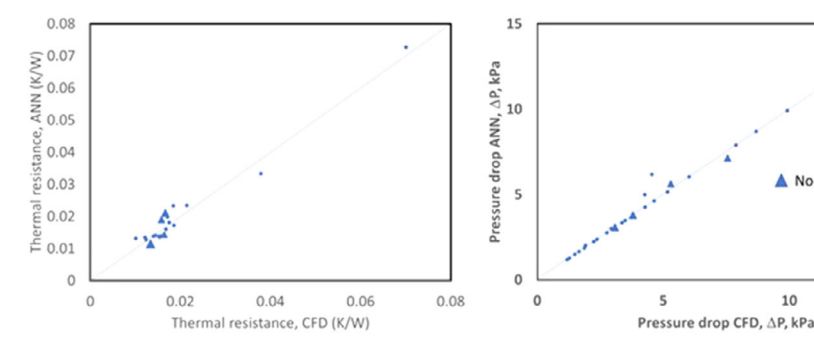


Fig. 21. Parity plot of the(a) Thermal resistance and (b) pressure drop from the network fitting for number of hidden neurons = 5 in a single hidden layer with R2=0.99. This indicated that the vale Ew is minimized. Points marked with the symbol " Δ " are the non-trained data.

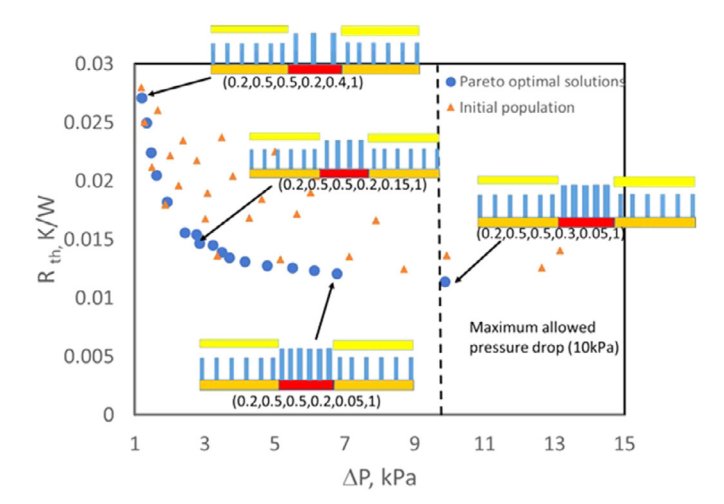


Fig. 22. Pareto optimal solutions obtained from the present study. The values in the parenthesis under each design schematic corresponds to $(t_f^{BG}, g_f^{BG}, h_f^{BG}, t_f^{HS}, g_f^{HS},$ and h_f^{HS}). The dashed lines indicate the pressure drop constraints.

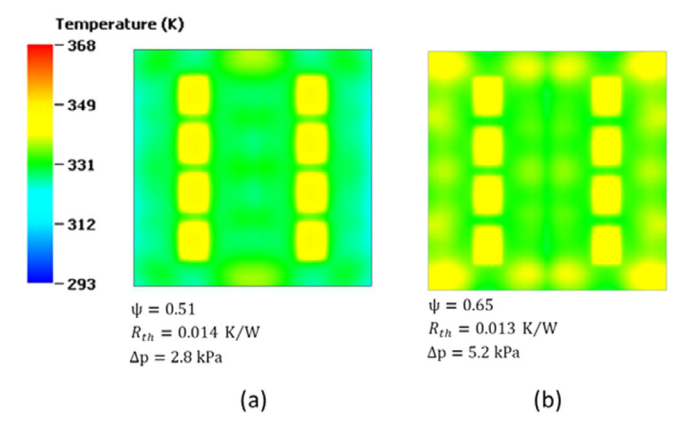


Fig. 23. Chip temperature profile of the (a) non-uniform improved design obtained in Section 4.2 and (b) final optimal design (lowest thermal resistance).

reducing fin gap on the hotspot (g_f^{HS}) as in the minimum value of g_f^{HS} (0.1 mm), t_f^{HS} does not affect thermal performance anymore.

vi. Both g_f^{HS} and t_f^{HS} have remarkable effects on the pressure drop of the system. The sensitivity of the pressure drop to g_f^{HS} and t_f^{HS} increases by decreasing g_f^{HS} .

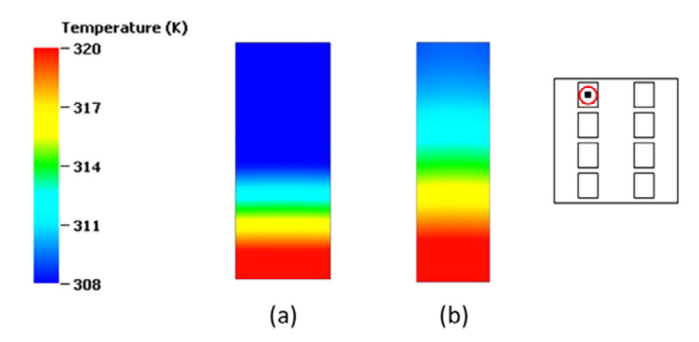


Fig. 24. Hotspot fin temperature profiles for (a) non-uniform improved design obtained in Section 4.2 and (b) final optimal design.

- vii. The cases with zero gap between the top of the fins on the hotspots and the lid present the optimal thermo-hydraulic performance.
- viii. Multi-inlet manifold with inlets on the top of each hotspot provides a much higher thermal and hydraulic performance than the single-inlet design.
- ix. A fin profile with 1mm and 0.5mm height on the hotspot and background regions, respectively, offers optimal thermohydraulic performance.
- x. A Bayesian based supervised learning algorithm was demonstrated for the problem under consideration.
- xi. An optimal thermal resistance of 0.2 K.cm²/W was achieved in this study under constrained pressure drop conditions.

This study paves way for future system energy efficient design and optimization of embedded cooling system in the form of printed fins directly on the chip. Eqs. (1)–((4)).

Declaration of Competing Interest

The authors declare that they have no known competing financial interests or personal relationships that could have appeared to influence the work reported in this paper.

Acknowledgment

This work is supported by SRC (Task 2878.006). S.N.S. acknowledges the NSF Award IIP-1738793 and the Integrated Electronics Engineering Center (IEEC) at the State University of New York at Binghamton. The IEEC is a New York State Center for Advanced Technology with funding from New York State through the Empire State Development Corporation. The authors would like to acknowledge Future Facilities for their solver package of 6SigmaET and its support through the course of this study.

References

- R.W. Knight, D.J. Hall, J.S. Goodling, R.C. Jaeger, Heat sink optimization with application to microchannels, IEEE Trans. Compon. Hybrids Manuf. Technol. 15 (1992) 832–842, doi:10.1109/33.180049.
- [2] W. Qu, I. Mudawar, Experimental and numerical study of pressure drop and heat transfer in a single-phase micro-channel heat sink, Int. J. Heat Mass Transf. 45 (2002) 2549–2565, doi:10.1016/S0017-9310(01)00337-4.
- [3] X. Xie, Z.J. Liu, Y.L. He, W.Q. Tao, Numerical study of laminar heat transfer and pressure drop characteristics in a water-cooled minichannel heat sink, Appl. Therm. Eng. 29 (2009) 64–74, doi:10.1016/j.applthermaleng.2008.02.002.
- [4] A. Alhusseny, A. Al-Fatlawi, Q. Al-Aabidy, A. Nasser, N. Al-Zurfi, Dissipating the heat generated in high-performance electronics using graphitic foam heatsinks cooled with a dielectric liquid, Int. Commun. Heat Mass Transf. 127 (2021) 105478, doi:10.1016/j.icheatmasstransfer.2021.105478.
- [5] D.B. Tuckerman, R.F.W. Pease, High-performance heat sinking for VLSI, IEEE Electron Device Lett. 2 (1981) 126–129, doi:10.1109/EDL.1981.25367.
- [6] D. Yang, Y. Wang, G. Ding, Z. Jin, J. Zhao, G. Wang, Numerical and experimental analysis of cooling performance of single-phase array microchannel heat sinks with different pin-fin configurations, Appl. Therm. Eng. (2017) 1547–1556.
- [7] L. Chai, G.D. Xia, H.S. Wang, Parametric study on thermal and hydraulic characteristics of laminar flow in microchannel heat sink with fan-shaped ribs on sidewalls part 1: heat transfer, Int. J. Heat Mass Transf. 97 (2016) 1069–1080, doi:10.1016/j.ijheatmasstransfer.2016.02.077.
- [8] L. Lin, J. Zhao, G. Lu, X.D. Wang, W.M. Yan, Heat transfer enhancement in microchannel heat sink by wavy channel with changing wavelength/amplitude, Int. J. Therm. Sci. C (2017) 423–434, doi:10.1016/j.ijthermalsci.2017.05.013.
- [9] Y. Hadad, B. Ramakrishnan, R. Pejman, S. Rangarajan, P.R. Chiarot, A. Pattamatta, B. Sammakia, Three-objective shape optimization and parametric study of a micro-channel heat sink with discrete non-uniform heat flux boundary conditions, Appl. Therm. Eng. 150 (2019) 720–737, doi:10.1016/j.applthermaleng.2018.12.128.
- [10] Y. Hadad, S. Rangararajan, K. Nemati, B. Ramakrishnann, R. Pejman, P.R. Chiarot, B. Sammakia, Performance analysis and shape optimization of a water-cooled impingement micro-channel heat sink including manifolds, Int. J. Therm. Sci. 148 (2020) 106145, doi:10.1016/j.ijthermalsci.2019.106145.
- [11] Y. Hadad, N. Fallahtafti, L. Choobineh, C.H. Hoang, V. Radmard, P.R. Chiarot, B. Sammakia, Performance analysis and shape optimization of an impingement microchannel cold plate, IEEE Trans. Compon. Packag. Manuf. Technol. 10 (2020) 1304–1319, doi:10.1109/TCPMT.2020.3005824.
- [12] V. Pangracious, Z. Marrakchi, H. Mehrez, Three-Dimensional Integration: A More Than Moore Technology, in: Three-Dimensional Design Methodologies for Tree-based FPGA Architecture, Springer International Publishing. 2015. 10.1007/978-3-319-19174-4_2. https://www. springerprofessional.de/en/three-dimensional-integration-a-more-thanmoore-technology/2452734.
- [13] T.Y. Chiang, S.J. Souri, C.O. Chui, K.C. Saraswat, Thermal analysis of heterogeneous 3D ICs with various integration scenarios, in: Proceedings of the International Electron Devices Meeting. Technical Digest (Cat. No.01CH37224), 2001, pp. 31.2.1–31.2.4, doi:10.1109/IEDM.2001.979599.
- [14] L. Choobineh, A. Jain, Determination of temperature distribution in three-dimensional integrated circuits (3D ICs) with unequally-sized die, Appl. Therm. Eng. 56 (2013) 176–184, doi:10.1016/j.applthermaleng.2013.03.006.
- [15] L. Choobineh, A. Jain, An explicit analytical model for rapid computation of temperature field in a three-dimensional integrated circuit (3D IC), Int. J. Therm. Sci. 87 (2015) 103–109, doi:10.1016/j.ijthermalsci.2014.08.012.
- [16] S. Rangarajan, Y. Hadad, L. Choobineh, B. Sammakia, Minimizing temperature nonuniformity by optimal arrangement of hotspots in vertically stacked threedimensional integrated circuits, J. Electron. Packag. 142 (2020), doi:10.1115/1. 4047471
- [17] Y. Hadad, V. Radmard, S. Rangarajan, M. Farahikia, G. Refai-Ahmed, P.R. Chiarot, B. Sammakia, Minimizing the effects of on-chip hotspots using multiobjective optimization of flow distribution in water-cooled parallel microchannel heatsinks, J. Electron. Packag. 143 (2020), doi:10.1115/1.4048590.
- [18] D. Ansari, K.Y. Kim, Hotspot thermal management using a microchannel-pinfin hybrid heat sink, Int. J. Therm. Sci. 134 (2018) 27–39, doi:10.1016/j.ijthermalsci. 2018.07.043.
- [19] D. Ansari, K.Y. Kim, Hotspot management using a hybrid heat sink with stepped pin-fins, Numer. Heat Transf. Part A Appl. 75 (2019) 359–380, doi:10. 1080/10407782.2019.1599272.
- [20] S. Feng, Y. Yan, H. Li, L. Zhang, S. Yang, Thermal management of 3D chip with non-uniform hotspots by integrated gradient distribution annular-cavity micro-pin fins, Appl. Therm. Eng. 182 (2021) 116132, doi:10.1016/j.applthermaleng.2020.116132.
- [21] D. Lorenzini, C. Green, T.E. Sarvey, X. Zhang, Y. Hu, A.G. Fedorov, M.S. Bakir, Y. Joshi, Embedded single phase microfluidic thermal management for non-uniform heating and hotspots using microgaps with variable pin fin clustering, Int. J. Heat Mass Transf. 103 (2016) 1359–1370, doi:10.1016/j.ijheatmasstransfer. 2016.08.040.
- [22] T.E. Sarvey, Y. Hu, C.E. Green, P.A. Kottke, D.C. Woodrum, Y.K. Joshi, A.G. Fedorov, S.K. Sitaraman, M.S. Bakir, Integrated circuit cooling using heterogeneous micropin-fin arrays for nonuniform power maps, IEEE Trans. Compon. Packag. Manuf. Technol. 7 (2017) 1465–1475, doi:10.1109/TCPMT.2017.2704525.

- [23] C.A. Rubio-Jimenez, S.G. Kandlikar, A. Hernandez-Guerrero, Performance of online and offset micro pin-fin heat sinks with variable fin density, IEEE Trans. Compon. Packag. Manuf. Technol. 3 (2013) 86–93, doi:10.1109/TCPMT.2012. 2225143
- [24] C.A. Rubio-Jimenez, S.G. Kandlikar, A. Hernandez-Guerrero, Numerical analysis of novel micro pin fin heat sink with variable fin density, IEEE Trans. Compon. Packag. Manuf. Technol. 2 (2012) 825–833, doi:10.1109/TCPMT.2012.2189925.
- [25] C. Bachmann, A. Bar-Cohen, Hotspot remediation with anisotropic thermal interface materials, in: Proceedings of the 11th Intersociety Conference on Thermal and Thermomechanical Phenomena in Electronic Systems, 2008, doi:10. 1109/ITHERM.2008.4544276.
- [26] X. Hao, B. Peng, G. Xie, L. Chen, Efficient on-chip hotspot removal via combination of thermoelectric cooler and mini-channel heat sink, Appl. Therm. Eng. 100 (2016), doi:10.1016/j.applthermaleng.2016.01.131.
- 100 (2016), doi:10.1016/j.applthermaleng.2016.01.131.
 [27] P. Wang, B. Yang, A. Bar-Cohen, Mini-contact enhanced thermoelectric coolers for on-chip hot spot cooling, Heat Transf. Eng. 30 (2009) 736–743, doi:10.1080/ 01457630802678391.
- [28] G. Bulman, P. Barletta, J. Lewis, N. Baldasaro, M. Manno, A. Bar-Cohen, B. Yang, Superlattice-based thin-film thermoelectric modules with high cooling fluxes, Nat. Commun. 7 (2016) 10302, doi:10.1038/ncomms10302.
- [29] A. Azizi, M.A. Daeumer, S.N. Schiffres, Additive laser metal deposition onto silicon, Addit. Manuf. 25 (2019) 390–398, doi:10.1016/j.addma.2018.09.027.
 [30] A. Azizi, M.A. Daeumer, J.C. Simmons, B.G. Sammakia, B.T. Murray,
- [30] A. Azizi, M.A. Daeumer, J.C. Simmons, B.G. Sammakia, B.T. Murray, S.N. Schiffres, Additive laser metal deposition onto silicon for enhanced microelectronics cooling, in: Proceedings of the IEEE 69th Electronic Components and Technology Conference (ECTC), 2019, pp. 1970–1976, doi:10.1109/ ECTC.2019.00302.
- [31] V. Radmard, Y. Hadad, A. Azizi, S. Rangarajan, C.H. Hoang, C. Arvin, K. Sikka, S.N. Schiffres, B. Sammakia, Direct micro-pin jet impingement cooling for high heat flux applications, in: Proceedings of the 36th Semiconductor Thermal Measurement, Modeling Management Symposium (SEMI-THERM), 2020, pp. 1–9, doi:10.23919/SEMI-THERM50369.2020.9142864.
- [32] V. Radmard, Y. Hadad, S. Rangarajan, C.H. Hoang, N. Fallahtafti, C.L. Arvin, K. Sikka, S.N. Schiffres, B.G. Sammakia, Multi-objective optimization of a chipattached micro pin fin liquid cooling system, Appl. Therm. Eng. 195 (2021) 117187, doi:10.1016/j.applthermaleng.2021.117187.
- [33] C.S. Sharma, M.K. Tiwari, S. Zimmermann, T. Brunschwiler, G. Schlottig, B. Michel, D. Poulikakos, Energy efficient hotspot-targeted embedded liquid cooling of electronics, Appl. Energy 138 (2015) 414–422, doi:10.1016/j. apenergy.2014.10.068.
- [34] R.V. Rao, K.C. More, J. Taler, P. Ocłoń, Dimensional optimization of a microchannel heat sink using Jaya algorithm, Appl. Therm. Eng. 103 (2016) 572–582, doi:10.1016/j.applthermaleng.2016.04.135.
- [35] K. Kulkarni, A. Afzal, K.Y. Kim, Multi-objective optimization of a double-layered microchannel heat sink with temperature-dependent fluid properties, Appl. Therm. Eng. 99 (2016), doi:10.1016/j.applthermaleng.2016.01.039.
- [36] N.H. Naqiuddin, L.H. Saw, M.C. Yew, F. Yusof, H.M. Poon, Z. Cai, H.S. Thiam, Numerical investigation for optimizing segmented micro-channel heat sink by Taguchi-Grey method, Appl. Energy 222 (2018) 437–450, doi:10.1016/j. apenergy.2018.03.186.
- [37] H. Lee, M. Kang, K.W. Jung, C.R. Kharangate, S. Lee, M. Iyengar, C. Malone, M. Asheghi, K. Goodson, H. Lee, An artificial neural network model for predicting frictional pressure drop in micro-pin fin heat sink, Appl. Therm. Eng. (2021), doi:10.1016/J.APPLTHERMALENG.2021.117012.
- [38] X. Xiang, Y. Fan, A. Fan, W. Liu, Cooling performance optimization of liquid alloys Galn y in microchannel heat sinks based on back-propagation artificial neural network, Appl. Therm. Eng. 127 (2017), doi:10.1016/j.applthermaleng. 2017.08.127
- [39] A. Ghaedi, Simultaneous prediction of the thermodynamic properties of aqueous solution of ethylene glycol monoethyl ether using artificial neural network, J. Mol. Liq. 207 (2015) 327–333, doi:10.1016/j.molliq.2015.04.015.
- [40] J. Mohammadpour, S. Husain, F. Salehi, A. Lee, Machine learning regression-CFD models for the nanofluid heat transfer of a microchannel heat sink with double synthetic jets, Int. Commun. Heat Mass Transf. 130 (2022) 105808, doi:10.1016/j.icheatmasstransfer.2021.105808.
- [41] R. Srikanth, P. Nemani, C. Balaji, Multi-objective geometric optimization of a PCM based matrix type composite heat sink, Appl. Energy 156 (2015) 703–714, doi:10.1016/j.apenergy.2015.07.046.
- [42] S. Rangarajan, C. Balaji, Phase Change Material-Based Heat Sinks: A Multi-Objective Perspective, 1st ed., CRC Press, Boca Raton, 2019.
- [43] Y. Amini, S.E. Habibi, Effects of multiple flexible vortex generators on the hydrothermal characteristics of a rectangular channel, Int. J. Therm. Sci. 175 (2022) 107454, doi:10.1016/j.ijthermalsci.2021.107454.
- [44] V. Semin, M. Bardsley, O. Rosten, C. Aldham, Application of a multilevel unstructured staggered solver to thermal electronic simulations, in: Proceedings of the 31st Thermal Measurement, Modeling Management Symposium (SEMI-THERM), 2015, pp. 287–292, doi:10.1109/SEMI-THERM.2015.7100174.
- [45] H.C. Chiu, R.H. Hsieh, K. Wang, J.H. Jang, C.R. Yu, The heat transfer characteristics of liquid cooling heat sink with micro pin fins, Int. Commun. Heat Mass Transf. 86 (2017) 174–180, doi:10.1016/j.icheatmasstransfer.2017.05.027.
- [46] L. Nakharintr, P. Naphon, S. Wiriyasart, Effect of jet-plate spacing to jet diameter ratios on nanofluids heat transfer in a mini-channel heat sink, Int. J. Heat Mass Transf. 116 (2018) 352–361, doi:10.1016/j.ijheatmasstransfer.2017.09.037.

- [47] P. Naphon, S. Klangchart, Effects of outlet port positions on the jet impingement heat transfer characteristics in the mini-fin heat sink, Int. Commun. Heat Mass Transf. 38 (2011) 1400–1405 INT Commun Heat Mass Trans, doi:10.1016/j.icheatmasstransfer.2011.08.017.
- [48] P. Naphon, L. Nakharintr, S. Wiriyasart, Continuous nanofluids jet impingement heat transfer and flow in a micro-channel heat sink, Int. J. Heat Mass Transf. 126 (2018) 924–932, doi:10.1016/j.ijheatmasstransfer.2018.05.101.
- [49] L. Nakharintr, P. Naphon, Magnetic field effect on the enhancement of nanofluids heat transfer of a confined jet impingement in mini-channel heat sink, Int. J. Heat Mass Transf. 110 (2017) 753-759, doi:10.1016/j.ijheatmasstransfer.2017. 03.078.
- [50] N.H. Naqiuddin, L.H. Saw, M.C. Yew, F. Yusof, T.C. Ng, M.K. Yew, Overview of micro-channel design for high heat flux application, Renew. Sustain. Energy Rev. 82 (2018) 901–914, doi:10.1016/j.rser.2017.09.110.
- [51] H.R. Upadhye, S.G. Kandlikar, Optimization of microchannel geometry for direct chip cooling using single phase heat transfer, Am. Soc. Mech. Eng. Digit. Collect. (2008) 679–685, doi:10.1115/ICMM2004-2398.
- [52] D.J.C. MacKay, Bayesian interpolation, Neural Comput. 4 (1992) 415–447, doi:10.1162/neco.1992.4.3.415.

- [53] F.Dan Foresee, M.T. Hagan, Gauss-Newton approximation to Bayesian learning, in: Proceedings of the International Conference on Neural Networks (ICNN'97), 3, 1997, pp. 1930–1935, doi:10.1109/ICNN.1997.614194.
- [54] K. Deb, A. Pratap, S. Agarwal, T. Meyarivan, A fast and elitist multiobjective genetic algorithm: NSGA-II, IEEE Trans. Evol. Comput. 6 (2002) 182–197, doi:10. 1109/4235.996017.
- [55] R. Srikanth, C. Balaji, Experimental investigation on the heat transfer performance of a PCM based pin fin heat sink with discrete heating, Int. J. Therm. Sci. 111 (2017) 188–203, doi:10.1016/j.ijthermalsci.2016.08.018.

Further reading

- [56] Y.J. Lee, P.S. Lee, S.K. Chou, Hotspot mitigating with obliquely finned microchannel heat sink—an experimental study, IEEE Trans. Compon. Packag. Manuf. Technol. 3 (2013) 1332–1341, doi:10.1109/TCPMT.2013.2244164.
- [57] P.S. Lee, S.V. Garimella, Hot-spot thermal management with flow modulation in a microchannel heat sink, Am. Soc. Mech. Eng. Digit. Collect. (2008) 643– 647, doi:10.1115/IMECE2005-79562.